ESR studies of O_2^- adsorbed on Ti supported surfaces: Analysis of motional dynamics

M. Shiotani,[a] G. Moro, and J. H. Freed

Baker Laboratory of Chemistry, Cornell University, Ithaca, New York 14850
(Received 8 September 1980; accepted 4 November 1980)

Temperature-dependent ESR spectra of O_2^- adsorbed on Ti ions supported on porous Vycor glass were observed over the range 4.2 to 400 °K. These spectra were obtained under normal high vacuum conditions as well as under UHV conditions ($P \leq 10^{-9}$ Torr) and are very well resolved. It was observed that the line position of the $\tilde{g}$ tensor component that is perpendicular to the internuclear axis of O_2^- remained constant with temperature, whereas the other two components of the $\tilde{g}$ tensor shift in position with temperature, and are accompanied by drastic line shape changes. This observation indicates that the molecular motion of O_2^- on the surface is highly anisotropic, consisting essentially of planar rotation about the axis perpendicular to the internuclear axis of O_2^- and parallel to the normal to the surface. Furthermore, the observation of nonequivalent ^{17}O hfs of O_2^- suggests that the internuclear axis of O_2^- might be tilted slightly from the surface and/or one oxygen is closer to the Ti^{4+}. The ESR line shapes were simulated for the different possible models: Brownian diffusion, jump diffusion (from weak jump to strong jump), approximate free diffusion, and discrete jump. It was found that the theoretical spectra calculated using the model of weak jump rotational diffusion best fit the observed spectra in the temperature range below 57.4 °K. However, in the temperature range above 57.4 °K, although the Brownian diffusion model seems the best among the models used, none of the present models used could successfully reproduce the observed line shapes. The rotational correlation time $\tau_{R\parallel}$ was found to range between $\sim 10^{-5}$ sec (below 14.5 °K) and 10^{-9} sec (263 °K). The values of $\tau_{R\parallel}$ depend strongly on the model used in the lower temperature range, but were essentially independent of model above 100 °K. The activation energy for rotational diffusion was estimated to be 0.5 kcal/mole above 100 °K. The line shape below 15 °K is independent of temperature, although the O_2^- spectrum appears to exhibit residual motional effects. This observation suggests that coherent quantum mechanical motion is predominant below 15 °K. This matter is discussed in some detail, and the appropriate theory to investigate quantum effects on the motional dynamics is outlined including possible isotope effects on the motion. Spectral observation of possible interaction between C_2H_4 and O_2^- on the surface is presented. Also discussed are the techniques for preparing samples with strong well-resolved signals and for removing the other types of O_2^- signals, which do not show significant temperature-dependent spectral changes.

I. INTRODUCTION

The superoxide ion O_2^- is one of the most extensively studied radical species because of its participation in a wide range of chemical and biochemical processes.[1] Since the first report of O_2^- formed on ZnO surfaces,[2] adsorbed oxygen on the surfaces of oxides, metal oxides, supported catalysts, and zeolites have been investigated using ESR, and various forms of adsorbed oxygen have been proposed.[3] Most of the studies have been carried out to characterize the adsorbed oxygen species and to elucidate the role of oxygen in the surface reaction for the catalytic oxidation of inorganic molecules, as well as the oxidation and oxidative dehydrogenation of hydrocarbons. However, only one study of the motional dynamics of O_2^- on a surface has previously been reported.[4]

Although a considerable number of studies were reported relating to motion of radicals adsorbed on solid surfaces,[5–10] the studies mostly have been limited to "qualitative" analysis of the ESR spectra in terms of the motion of the radical and the nature of the radical–surface interaction. As far as we know, there are no "quantitative" analyses on molecular dynamics of the ESR line shape, except for the study of slow molecular motion of O_2^- stabilized on metallic Ag supported on Vycor by means of saturation transfer (ST) ESR,[4] a more approximate analysis of ESR spectra from the hindered motion of NO_2 and ClO_2 adsorbed in synthetic zeolites,[11] and recent work on polyatomic peroxy radicals.[12]

We have found that one of the several species of O_2^- adsorbed on Ti^{4+} supported on porous Vycor glasses gives rise to temperature-dependent ESR spectra in the wide temperature range from 4.2 to 400 °K. The purpose of the present paper is to discuss a model for the motion of O_2^- adsorbed on Ti^{4+}/Vycor surfaces which is consistent with the observed temperature-dependent ESR line shape and thereby obtain insight into the dynamical structure of the adsorption site.

In our laboratory, the theory for slow motional ESR spectra has been extensively developed and has been successfully applied to ESR line shapes of the nitroxide free radical and the VO^{2+} ion in isotropic and anisotropic liquids.[13–16] The theory will be applied, in the present studies, to the analysis of the temperature-dependent ESR line shapes of O_2^- adsorbed on the surface. This, we believe, is an important application of the theory to molecular dynamics at the gas–solid interface.

In Secs. III A and III B, we will summarize our results on formation and characterization of various types of oxygen radicals O^- (I and II) and O_2^- (I, II, and III) adsorbed on partially reduced Ti ion supported on porous

[a] Permanent address: Faculty of Engineering, Hokkaido University, Sapporo 060, Japan.

 0021-9606/81/042616-25$01.00

Vycor glasses and compare them with the previous studies on similar systems. Also discussed are the techniques for preparing samples with strong well-resolved signals and for removing the other types of oxygen radicals which do not show significant temperature-dependent spectral changes. We show the ESR line shapes and ESR parameters of $^{16}O_2^-$(III) and $^{17}O_2^-$(III), the species that exhibits highly anisotropic motion. We also present a spectral observation of possible interaction between added C_2H_4 and this O_2^- on the surface.

In Sec. III C, the temperature-dependent line shape of $^{16}O_2^-$(III) is analyzed by detailed spectral simulation using our slow motional ESR spectral theory for different diffusion models[13] (Brownian diffusion, jump diffusion, and approximate free diffusion) and also a discrete jump model.[17] It will be shown from the simulation that the highly anisotropic motion of O_2^- is well approximated by planar rotational diffusion around an axis perpendicular to the internuclear axis of O_2^- and normal to the surface. Further, the weak jump model fits the observed spectra reasonably well in the lower temperature region. Implications of these results are then discussed.

Furthermore, the observation of a temperature-independent line shape below 15 °K and of isotope effects on the line shape is discussed in terms of "quantum effects" on the motions. Finally, our results of O_2^- on the Ti/Vycor system are compared with those of the Ag/Vycor system.[4]

II. EXPERIMENTAL

A. Sample preparation

The porous Vycor quartz glass (Corning Code No. 7930, controlled pore size of 40 Å) was supplied in a crushed form by Dr. J. Schreurs, Corning Glass Works. The crushed Vycor was cleaned in the manner of Clarkson,[18] i.e., the Vycor is pretreated with concentrated HNO_3 and rinsed thoroughly with distilled water. The Vycor is then evacuated, treated for 24 h with 1 atm O_2, evacuated, and then treated for 24 h with 1 atm H_2, followed by evacuation and heating at 550 °C in order to remove contaminants.

The Ti-containing samples were prepared by impregnation of Vycor by $TiCl_4$ (99.9%, Alfa Products) aqueous solution, in a manner similar to Kazansky's,[19] i.e., the clean Vycor of 0.8 g was immersed in a 0.04 M aqueous solution of $TiCl_4$. The mixture was allowed to stand for 24 h at room temperature, then filtered and dried in air overnight. Then the samples were dried at 80 °C and calcinated in air for several hours at 500 °C.

Before the adsorption of O_2 (Airco) and N_2O (Madison Gas Products) gases, the samples were placed into a 4 mm o.d. spectrosil ESR tube, evacuated, treated with 1 atm O_2 for 12 h, evacuated, reduced with 1 atm H_2 for 12 h, and finally evacuated to 10^{-6}–10^{-7} Torr at 500 °C. Ti^{4+} samples prepared in this manner were 0.18% by weight.[20]

The gases used in the experiments were purified twice through a liquid nitrogen cold trap. In the case of O_2, the vapor pressure of liquid O_2, twice distilled in vacuum, was used as the source of gaseous oxygen. The ^{17}O enriched O_2 (70 at% of ^{17}O, YEDAR R&D Co.) was used as received.

The Ti/Vycor samples were also prepared under ultrahigh vacuum (UHV) of $P \leq 10^{-9}$ Torr, using methods recently developed for ESR in our laboratory[21] in which the usual ESR sample tube was attached to the UHV system. Ultraviolet light irradiation was carried out either at room temperature or at liquid nitrogen temperature using a high pressure Hg lamp, without filter. The Vycor is known to transmit light of $\lambda > 220$ nm efficiently.

B. Measurement of ESR spectra

ESR spectra were recorded at X band with a Varian E-12 ESR spectrometer employing 100 kHz (or 10 kHz when needed) field modulation at a low enough amplitude so that no line shape distortion was observed. Microwave power was always adjusted so that no saturation occurred.

The sample temperature above liquid nitrogen temperature was controlled by a Varian E-257 variable temperature unit and measured with a copper-constantan thermocouple placed just above the sample. Moreover, the temperature of the sample was regulated within ±0.5 °K between 4.2 and 80 °K by means of an Oxford Instrument, ESR 9 continuous He gas flow cryostat.

The magnetic field was measured and calibrated with a Harvey-Wells meter. The microwave frequency was measured with a Systron-Donner electronic counter.

The gases were introduced to the pretreated Ti/Vycor sample already in the ESR cavity using either the ordinary high vacuum system of $P \simeq 10^{-6}$–10^{-7} Torr or the UHV system of $P \leq 10^{-9}$ Torr, which enabled us to detect *in situ* the change in concentration and in line shape of the radical formed as a function of gas concentration and time.

III. EXPERIMENTAL RESULTS AND DISCUSSION

A. Formation of several types of oxygen radicals

As described in Sec. I, the main interest in the present studies is to observe temperature-dependent spectra of O_2^-, stabilized on the surface of Ti-supported Vycor glass, and to discuss the molecular dynamics using the stochastic theory of spin relaxation in the slow motional region for different possible models, which have been developed in our laboratory.[12,13] However, in the present system, several types of oxygen radicals O_2^- and O^- are stabilized and observed at the same time, which leads to complications in the analysis of temperature-dependent spectra. Therefore, in order to study the molecular dynamics of O_2^-, it is helpful first to characterize the various species and then to eliminate experimentally the other species except for the one showing dramatic temperature-dependent line shapes. In this section, we will summarize our results on ESR spectra of radicals originating from O_2 adsorption on partially reduced Ti ion supported on porous Vycor glass

and compare them with the previous studies on similar systems.

Characteristic points in the present experiments may be summarized as follows:

(i) Although O_2 adsorption on reduced TiO_2 (Refs. 22–25) has been extensively studied, there are few papers[19] on supported Ti.

(ii) All spectra of O_2^- on oxides and supported catalysis in the previous studies were observed above liquid nitrogen temperature; however, in the present studies, the spectra were recorded below 77 down to 4.2 °K, which enhances the study of molecular dynamics of O_2^-.

(iii) The sample was also prepared under the UHV condition of $P \lesssim 10^{-9}$ Torr, which enabled us to check if formation, stability, and motion of O_2^- is affected by the degree of adsorption of gases on the Ti/Vycor surface.

(iv) Ti/Vycor samples with O_2 were irradiated by UV light, enabling us to observe several kinds of oxygen radicals. Furthermore, this irradiation greatly enhanced the yields of radicals coming from adsorbed O_2. This helped considerably to identify and analyze more easily the different radical spectra, especially $^{17}O_2^-$, because of the better signal-to-noise ratio.

1. O_2^- formation on Ti/Vycor (without UV irradiation)

The Ti/Vycor sample did not give any ESR signal before O_2 gas was admitted either at room temperature or at 77 °K, as is consistent with previous studies (the Ti/SiO_2 system contains 0.2 wt% Ti).[2] Nonobservation of Ti^{3+} is probably due to fast spin–lattice relaxation of Ti^{3+}, which has been discussed previously.[2]

When O_2 gas was introduced to the sample placed in the ESR cavity at room temperature, an ESR signal having g anisotropy started to grow with increasing O_2 gas pressure. The spectral intensity was found to increase with O_2 pressure up to 5 Torr and then to decrease gradually with a further increase in pressure at room temperature. It was also found that the intensity gradually decreased with time for samples containing O_2 gas above 2 Torr; the half-life was about 30 min at RT for a sample with 5 Torr O_2 gas. By evacuating O_2 at RT, the linewidth became slightly narrower and the resolution became better.

The observed spectrum consists of three different paramagnetic species: The first (species I) is the main signal with $g_1 = 2.0295$, $g_2 = 2.0093$, and $g_3 = 2.0034$ and the second species (species II) has $g_1' = 2.0223$. The third with $g = 1.9758$ can be attributed to a gas phase O_2 signal, which is readily confirmed by O_2 evacuation. The spectrum corresponding to the second species could be observed separately from the first when samples prepared by repeating the evacuation–oxidation–evacuation–reduction cycle at 500 °C twice were used. This result implies that the O_2^- adsorption sites are considerably affected by the extra treatment.

Based on the g values, these species I and II can be attributed to O_2^- stabilized at different sites of Ti/Vycor on the surface. The line shapes and apparent g values of both O_2^- species depend slightly on temperature between RT and 77 °K, but not drastically (cf. Table I). The species were stable at RT for several days but were made to decay by evacuating above 150 °C.

Shvets and Kazansky[19] have reported formation of two types of O_2^- on Ti supported on SiO_2 after O_2 admission at room temperature. Although this is similar to our observation, the g values of O_2^- on Ti/Vycor are significantly different from those reported by them (cf. Tables I and II). The g values of O_2^- (I) and O_2^- (II) are very close to those of O_2^- formed on the rutile type of TiO_2 and anatase type of TiO_2,[22,23] respectively (cf. Tables I and II). The above arguments indicate that a local structure, or coordination, of surface Ti ion might play an important role in shifting the g value, especially the largest g value whose direction is known to be parallel to the internuclear axis of O_2^-.[26] Although the crystal lattices of Vycor glass and TiO_2 are not isomorphous, it is natural to assume that the identity of the O_2^- is explained by the formation of mixed crystals of TiO_2 of the anatase and rutile types on the Vycor glass surfaces of the fresh sample.

In order to confirm the role of the Ti ion in the O_2^- stabilization, the same experiments were carried out using samples of pure Vycor without Ti ions. No ESR signal (except O_2 gas phase signal) was observed after O_2 admission into the Vycor sample at RT and 77 °K, as expected.

2. O_2^- and O^- formation on Ti/Vycor system (assisted by UV light)

O_2/Vycor system: Before considering the O_2/Ti/Vycor system, formation of paramagnetic species by UV irradiation of O_2/Vycor will be mentioned.

When the pure Vycor sample with 2 Torr O_2 was irradiated at 77 °K, the spectrum was composed of a superposition of several kinds of paramagnetic species, and the main peak at $g = 2.002$ may reasonably be attributed to O^-(I) based on the g value.[19] Upon warming the sample at RT for several minutes, most of the paramagnetic species decayed away and only one thermally stable species, whose concentration was less than one tenth of the original ones, was observed. The thermally stable species was found to be formed immediately after UV irradiation at 77 °K, but the intensity roughly doubles after the other species decay. This species showing large g anisotropy ($g_{max} = 2.0428$ at 77 °K) is probably O_2^- stabilized at Si^{4+} or impurities in the Vycor, such as a B^{3+} site, the latter ion being a minor component of the Vycor (3% B_2O_3 in Corning Brand Vycor Glass No. 7930).

Recently, Anpo *et al.*[27] have reported photoformation of O_2^- adsorbed on porous Vycor glass. As the temperature of UV irradiation was not described in Ref. 27, one cannot directly compare those results with the present results. However, if the O_2/Vycor were irradiated at RT, both results would be consistent with each other except for the g values of the spectrum (they reported $\bar{g} = 2.0310$, 2.0109, 2.0053). The reason why different types of O_2^- were observed is not known at present, but it probably comes from the difference in local

TABLE I. ESR parameters of O_2^-, O^- species formed on Ti/Vycor system (present studies).

Species	Temperature	g value g_1	g_2	g_3	g_{av}	Notes
O_2^-(I)	RT	2.0295	2.0093	2.0034	2.0141	O_2–Ti/Vycor, adsorption at RT
	77 °K	2.0305	2.0088	2.0027	2.0140	
O_2^-(I′)	RT	2.0297	2.0090	2.0030	2.0139	O_2–Ti/Vycor, UV (257 mm) without filter at RT or 77 °K (formed upon warming to RT)
	77 °K	2.0300	2.0090	2.0022	2.0137	
O_2^-(II)	RT	2.0223	2.0093	2.0037	2.0118	O_2–Ti/Vycor
	77 °K	2.0237	2.0094	2.0035	2.0122	Stable at RT
O_2^-(III)	77 °K	2.0260	2.0092	2.0035	2.0129	O_2–Ti/Vycor, UV at RT or 77 °K. Rather unstable at RT (slowly decaying)
	36 °K	2.0268	2.0092	2.0027	2.0129	
		A_1	A_2	A_3		
		< 3 G	< 3 G	74.9 G 80.3 G		^{17}O hyperfine tensor
	4.2 °K	2.0271	2.0092	2.0025	2.0129	
O_2^-(III′)	77 °K	2.0256	2.0092	2.0039	2.0129	N_2O–Ti/Vycor, UV at 77 °K keeping the sample at RT for 20 h—stable at RT
O^-(I)	RT	unstable at RT				O_2–Ti/Vycor, UV at 77 °K
	77 °K	$g_{\parallel}$ = ?		$g_{\perp}$ = 2.0020		Probably $g_{\parallel} > g_{\perp}$
O^-(II)	RT	Undetectable because of line broadening				
	77 °K	$g_{\parallel}$ = ?		$g_{\perp}$ = 2.0455		Probably $g_{\perp} > g_{\parallel}$. O_2 or N_2O–Ti/Vycor, UV at 77 °K

structure of O_2^- trapping sites, depending on the sample preparation processes.

Further studies on thermally unstable species are currently under way.

O_2/Ti/*Vycor system*: Ti/Vycor with several Torr of O_2 (usually 2 Torr) was irradiated at 77 °K or room temperature using a high pressure Hg lamp without filter. A new O_2^- signal [O_2^-(I) (see ESR parameters in Table I)], appeared after several minutes of irradiation at 77 °K, together with the same signals observed in the absence of Ti ions. One example of the ESR spectrum is shown in Fig. 1(A), in which the weak signal, probably one type of O^- [O^-(I)] from the O_2/Vycor being observed overlapping at the band marked by an asterisk.

Upon warming the sample to room temperature for several minutes, the signals in the O_2/Vycor disappeared completely, the O_2^-(III) being slightly decreased in intensity (about 30% or 40%). However, new signals at $g = 2.0455$ and $g = 2.0303$ appeared after recooling the sample to 77 °K [cf. Fig. 1(B)].

The signal at $g = 2.0445$ has not been reported in previous studies on adsorption of O_2 in either Ti/SiO_2 (Ref. 19) or TiO_2 (Refs. 22–25) systems. However, the g value is very close to g_1 of O^- on MgO.[28] Therefore, it is reasonable to attribute this species to one type of O^- [O^-(II)] stabilized at a preferred site (Ti^{4+} may play an important role for the stabilization because the corresponding species could not be observed for samples without Ti), with O^-(I) or O_2^-(III) probably serving as a precursor of O^-(II).

The signal at $g = 2.0303$ is easily attributed to g_1 of O_2^-(I) mentioned above. This species is formed immediately after UV irradiation at 77 °K; the intensity relative to O_2^-(III) becomes larger after warming the sample at RT because of the slight decrease of O_2^-(III).

When the sample is observed at RT, the spectrum is considerably different from that at 77 °K. Although the resonance position of O_2^-(III) remains almost constant, the band corresponding to $g = 2.0455$ disappeared at RT, the line shape having changed drastically. This change was reversible between 77 °K and RT. These results indicate that (1) nonobservation of O^-(II) at RT is probably due to line broadening and (2) the line shape comes predominantly from that of O_2^-(III).

Furthermore, the thermal stability of O_2^-(I) was found to be higher than that of O^-(II) and O_2^-(III) so that the O_2^-(I) spectrum could be observed separately from that of O^-(II) and O_2(III), which decay out after keeping the sample at RT for about 10 days. The line shape did not change significantly on varying the temperature between RT and 77 °K. The best-fit simulated spectrum for O_2^-(I) at 77 °K gave the g values of $g_1 = 2.0300$, $g_2 = 2.0090$, and $g_3 = 2.0022$ and large orientation-dependent Lorentzian linewidths $1/T_2^0$ of 2.5, 0.5, and 0.85 G. Two possible explanations for the linewidths are as follows: (1) There are residual molecular motional effects on the spectrum, a matter to be discussed in the next section, or (2) an inhomogeneous distribution of adsorption sites which result in a superposition of the spectra having slightly different g values. It should be noted that orientation-dependent intrinsic linewidths

TABLE II. ESR parameters of oxygen radical ions formed on Ti/SiO_2, TiO_2, and other oxides (previous studies).

Species	Reference	System	Temp.	g value				hf splitting (G)			Notes
				g_1	g_2	g_3	g_{av}	A_1	A_2	A_3	
O_2^-	22	O_2/TiO_2 (anatase)	77 °K	2.024 2.020	2.009 2.009	2.003 2.003	2.012 2.011	... ...	... ...	... ...	← O_2^- (II)
O_2^- (A)	19	$O_2/Ti/SiO_2$	77 °K	2.020 ± 0.001	2.009 ± 0.001	2.003 ± 0.001	2.011	...	...	...	
O_2^- (B)	19	$O_2/Ti/SiO_2$	77 °K	2.026	2.009	2.003	2.013	...	...	...	← O_2^- (III)
O^-	19	$N_2O/Ti/SiO_2$ (UV)	77 °K	$g_{\parallel}=2.011$, $g_{\perp}=2.002$			2.005	...	...	...	← O^- (I)
O_2^- (A1)	23	O_2TiO_2 (anatase)	77 °K	2.025	2.009	2.003	2.012	...	...	77	← O_2^- (III′)
O_2^- (A2)$_1$	23	O_2/TiO_2 (anatase)	77 °K	2.024	2.009	2.003	2.012	...	...	77	← O_2^- (III)
O_2^- (A2)$_2$	23	O_2/TiO_2 (antase)	77 °K	2.020	2.009	2.003	2.011	...	...	77	
O_2^- (R)$_1$	23	O_2/TiO_2 (rutile)	77 °K	2.030	2.008	2.004	2.014	...	...	76	← O_2^- (I)
O_2^- (R)$_2$	23	O_2/TiO_2	77 °K	2.020	2.009	2.003	2.011	...	...	72	
O^-	28	N_2O/MgO (UV)	77 °K	$g_{\parallel}=2.041$, $g_{\perp}=2.0016$				...	...	...	← O^- (II)
O_2^-	30	$O_2/W/SiO_2$	77 °K 418 °K	2.0266 $g_{\parallel}=2.007$, $g_{\perp}=2.018$	2.0097	2.0042	2.0135 2.014	... ...	... ...	74 ...	← close to O_2^- (III) or (III′)
O_2^- (A′)	25	O_2/TiO_2	RT	2.019	2.010	2.005	2.011	...	...	...	
O_2^- (B′)	25	O_2/TiO_2	RT	2.023	2.010	2.005	2.013	...	...	...	
O_2^- (C′)	25	O_2/TiO_2	RT	2.026	2.010	2.005	2.014	...	...	...	
O_2^-	24	O_2/TiO_2 (UV)	77 °K	2.021	2.009	2.001	2.010	...	...	...	
O_3^-	24	O_2/TiO_2 (UV)	77 °K	2.014	2.009	2.003	2.008	...	...	...	
O_3^{3-}	24	O_2/TiO_2 (UV)	77 °K	$g_{\parallel}=2.008$,	$g_{\perp}=2.001$		2.003	...	...	...	
O_2–CO^-	24	O_2/TiO_2+CO	77 °K	2.0465	2.006	2.001	2.0178	...	...	...	
O_2^-	4	$O_2/Ag/Vycor$	RT	2.028	2.0089	2.0041	2.0137	...	...	...	← close to O_2^- (I)
O_2^-	18	$O_2/Ag/Vycor$	RT	2.034	2.0115	2.0042	2.0166	...	...	...	
O_2^-	31	O_2/MgO	77 °K	2.0777	2.0089	2.0018	2.0295	15 ± 2	0 ± 4	77 ± 2	
O_2^-	32	O_2/ZnO	77 °K	2.0519 ~ 2.0424	2.0090	2.0024	2.0211	15 ± 4	0 ± 5	80 ± 2	
O_2^-	33	O_2/SnO	77 °K	2.024	2.009	2.0036	2.0122	...	...	80.5	
O_2^-	34	$O_2/CaO_2/SiO_2$	77 °K	2.028	2.0158	2.0109	2.0182	...	75	...	
O_2^-: nonequivalent oxygen nuclei											
O_2^-	35	$O_2/Mo/SiO_2$	77 °K	2.018	2.010	2.004	2.011	...	...	69 ± 1 82 ± 1	
	35	O_2/Zeolite	77 °K	2.038	2.009	2.002	2.016	...	...	63 ± 1 82 ± 1	
O_2^-	36	O_2/MgO	77 °K	2.0777	2.0089	2.0018	2.0295	...	...	76 78	
O_2^-	37	$O_2/Mo/SiO_2$	77 °K	2.0176	2.0098	2.0042	2.0105	...	...	72 85	
	37	$O_2/Mo/Al_2O_3$	77 °K	2.0170	2.103	2.0045	2.0415	...	...	77 80	

have been observed for very viscous liquid samples.[12]

The UV irradiated Ti/Vycor with O_2 at RT gave O_2^-(I), O_2^-(III), and O^-(II), but not O^-(I). The O_2^-(III) decays and only the signals of O_2^-(I) and O^-(II) are observed after keeping the sample at RT for 1 week.

3. O^- and O_2^- formation by decomposition of N_2O on Ti/Vycor surface using UV light

No signal was observed after admission of N_2O to the partially reduced Ti/Vycor sample at RT. When a sample containing 2 Torr N_2O was irradiated at 77 °K for several minutes, a strong signal due to O_2^-, type III [O_2^-(III)] appeared together with a weak signal having a partially resolved structure at the $g=2.0027$ region. This observation is very close to that reported by Shvets and Kazansky[19] for the Ti/SiO_2 system. According to these authors, the latter signal is attributed to O^- formed by light decomposition of N_2O and reaction of the nascent O with Ti^{3+}:

$$N_2O \xrightarrow{h\nu} N_2 + O ,$$

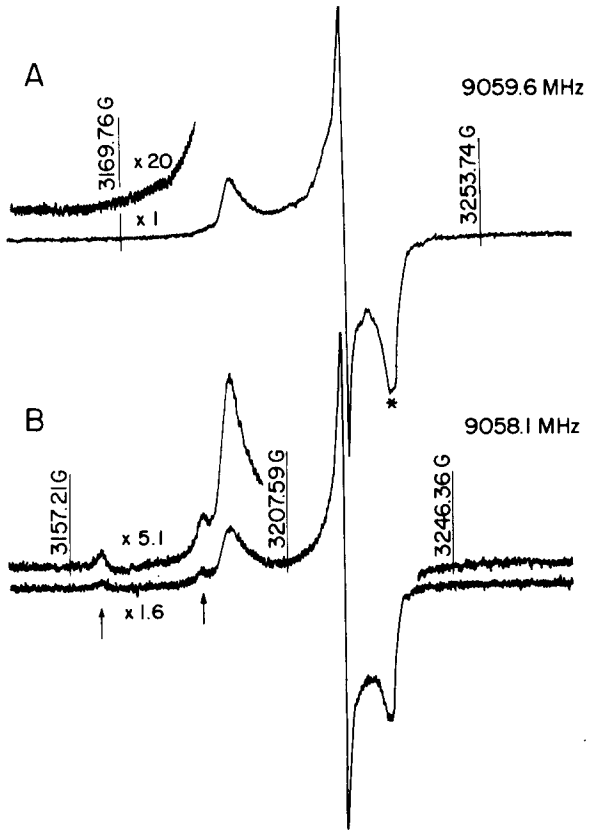

FIG. 1. ESR spectra of UV irradiated Ti supported Vycor with 2 Torr O_2. The UV irradiation was carried out at 77 °K for 10 min. The spectra (A) and (B) were recorded at 77 °K immediately after UV irradiation and after warming the sample at room temperature for 5 min, respectively. New bands appearing after annealing the sample are marked as arrows (↑) in (B).

$$O + Ti^{3+} \rightarrow [Ti^{4+}O^-]$$

On the other hand, step one could form an excited $(N_2O)^*$ which then reacts with Ti^{3+} to give the product. However, alternative reaction schemes are also possible, e.g.,

$$Ti^{3+} \xrightarrow{h\nu} Ti^{4+} + e \ ,$$

$$e^- + N_2O \rightarrow N_2 + O^-$$

to form the O^-.

Upon warming the sample to RT, the "O^-" signal decayed and was replaced by a signal at $g = 2.0455$, which is attributable to O^-(II). Interestingly, in this system, the O_2^-(II) species was more stable than that for the O_2/Ti/Vycor system and the g values were slightly changed after keeping the sample at RT for 24 h [O_2^-(III′), see Table I]. Furthermore, no signal from O_2^-(I) was observed.

For the formation of O_2^- on the surface, the following reaction schemes may be possible:

$$N_2O \xrightarrow{h\nu} N_2O^* \ ,$$

$$N_2O^* + N_2O \rightarrow N_2 + O_2 \ ,$$

and/or

$$O^- + O_2 \rightarrow O_2^- + O \ ,$$

$$O_2^- + Ti^{4+} \rightarrow (Ti^{4+} - O_2^-) \ .$$

B. ESR spectrum of type III O_2^-

As described in the previous section, the spectrum of O_2^-(III) was observed together with the other weak signals after UV irradiation of Ti/Vycor with O_2 or N_2O. We are especially interested in the O_2^-(III) species because the line shape of O_2^-(III) depends drastically on temperature. In order to analyze the temperature-dependent spectra by means of our theory for slow motional ESR spectra, it is extremely helpful to observe only the spectrum of O_2^-(III) separately from the others. Thus, several possible ways were tried to eliminate the other paramagnetic species. Finally, we found the conditions that give only O_2(III), viz., the Ti/Vycor sample was prepared by repeating the cycle several times of first outgasing, then oxidation with 1 atm O_2, then outgasing, followed by reduction with 1 atm H_2 and outgasing. Then the sample with several Torr of O_2 was UV irradiated at 77 °K and observed after warming to RT in order to cause decay of the unstable species trapped on the pure Vycor. Thus, only the O_2^-(III) spectrum was observed without formation of the other species O_2^-(I) and O^-(II). The "aged" sample was also found to be less active than the "fresh" sample with respect to the other type of O_2^- formation; no signal attributable to the O_2^- species O_2^-(I) and O_2^-(II) was observed after admission of O_2 gases at either RT or 77 °K. It should be noted that Clarkson and Civillo[18] had observed a similar effect of "surface aging" on their Ag supported Vycor glass.

A series of temperature-dependent ESR spectra of O_2^-(III) were observed in the temperature ranges between 4.2 °K and RT and are shown in Fig. 2. The species decayed out at around 150 °C under vacuum.

In order to record an accurate ESR spectrum, especially at 4.2 °K, particular attention must be paid to the field modulation frequency, its amplitude, and microwave power. ESR spectra at 4.2 °K were recorded employing 100 kHz field modulation at low enough amplitude (generally less than 0.1 G) that no line shape distortion was observed. It was found that saturation started to occur above the low microwave power of 0.25 mW incident. Using different modulation frequencies of 25 and 10 kHz, any line shape distortion was carefully checked out.

The line shape changes were found to be reversible with temperature between 4.2 °K and RT. The temperature-dependent spectra were recorded for the sample evacuated to 10^{-6} Torr at RT after O_2^- formation, since the O_2 gas in the sample contributed a slight linewidth broadening probably due to spin exchange.

Why did the O_2^-(I) and O_2^-(II) species not form on the aged sample? We offer the following possibility: formation of microcrystal TiO_2 of the anatase and rutile types on the Vycor surface are expected to yield stabilization sites for the O_2^-(I) and O_2^-(II) as mentioned above. During repeated annealing of the sample, these microcrystals might diffuse into the Vycor SiO_2 lattice, probably replacing Si atoms in their lattice sites with Ti.

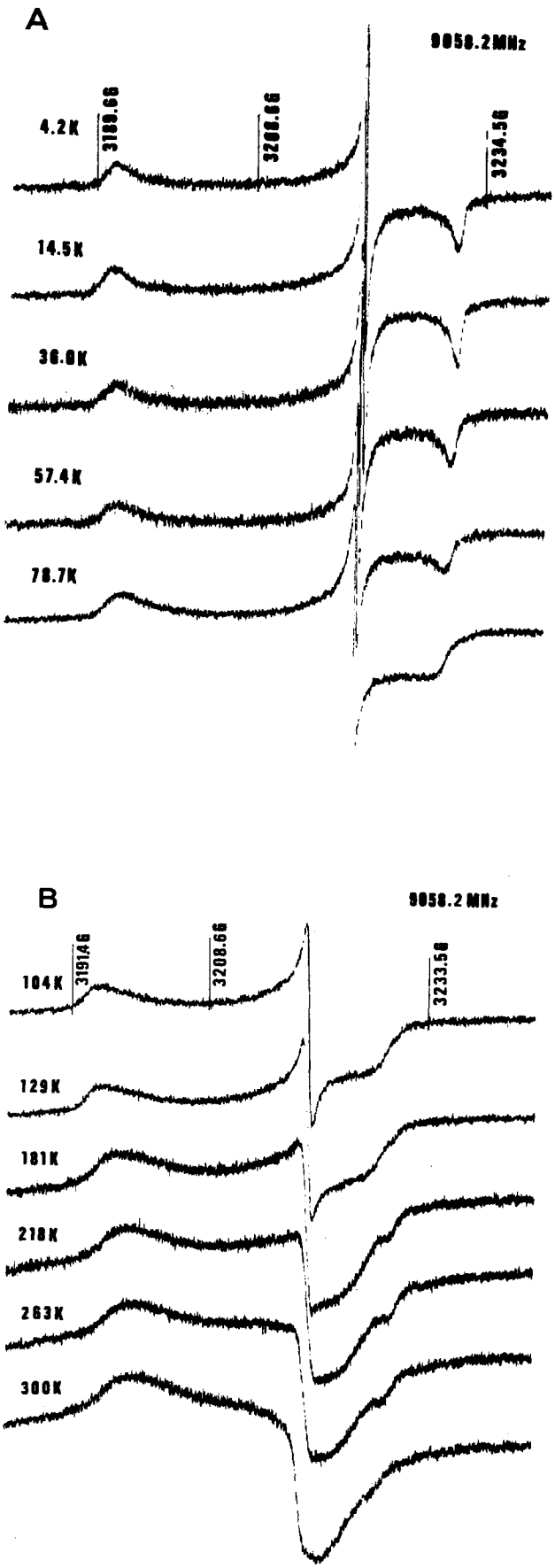

FIG. 2. Temperature-dependent ESR spectra of O_2^-(III): (A) below 80 °K; (B) above 80 °K. The "aged" sample (see details in the text) was used to observe only the O_2^-(III) species.

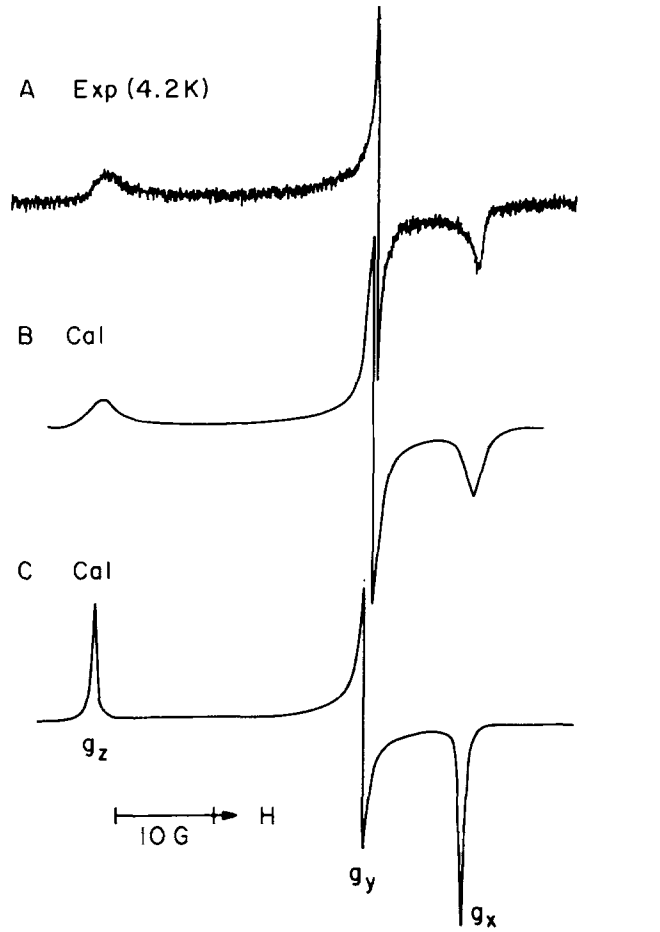

FIG. 3. Experimental spectrum of O_2^-(III) at 4.2 °K (A) and calculated ones (B) and (C) by the rigid limit program in order to determine the g-tensor components precisely. The spectrum (B) best fit the observed one, with parameters $g_x = 2.0025$, $g_y = 2.0092$, $g_z = 2.0271$, $1/T_{2x}^0 = 0.95$ G, $1/T_{2y}^0 = 0.18$ G, $1/T_{2z}^0 = 1.35$ G, and a Lorentzian line shape. The spectrum (C) was calculated using an orientation independent linewidth $1/T_{2x,y,z}^0 = 0.2$ G. The other parameters were the same as in (B).

Thus, these crystals could no longer exist on the Vycor surface.

1. ESR parameters of O_2^-(III)

In order to determine accurately the ESR parameters, i.e., the g values and intrinsic linewidth, the ESR simulation was carried out using a rigid limit simulation program based on the assumption that the spectra at 4.2 and 36 °K are in the rigid limit. The best fit simulation spectrum (B) is shown together with the observed one (A) at 4.2 °K in Fig. 3. The parameters used are given in the figure caption. A large orientation-dependent linewidth was needed to simulate the spectra. the intrinsic linewidth of Lorentzian line shape at the largest g values of 2.0271 (at 4.2 °K) and 2.0268 (at 36 °K) being about eight and nine times larger than that at $g = 2.0092$ for the spectra observed at 4.2 and 36 °K, respectively. This orientation-dependent linewidth is much larger than that usually observed in the rigid limit spectra (see, for example, Ref. 12). Therefore, it appears reasonable to attribute the large orienta-

tion-dependent linewidth to a residual molecular motion, i.e., it appears that even at 4.2 °K, the O_2^-(III) molecular ion is not in the rigid state on the surface but in a mobile state. This will be the subject of the following section. It should be noted that the g values and the line shape are identical for 14.5 and 4.2 °K. This implies that the molecular motion of O_2^- is independent of temperature below about 15 °K.[29]

2. Comparison with previous work on O_2^-(III)

Almost identical species to the present O_2^-(III) have been reported by two independent groups (Shvets and Kazansky[19] and Kazusaka *et al.*[30]). Although the samples used by them, viz., Ti/SiO_2 containing 0.2 wt% Ti ion[19] and W/SiO_2,[30] are different from ours, we believe that the reported oxygen molecular ions are almost identical to the present O_2^-(III) based on the g values (see Tables I and II) and the temperature-dependent line shape [cf. Fig. 3 of Ref. 19(a) and Fig. 1 of Ref. 30].

The experimental results of the previous workers, characteristic of Ti/SiO_2 containing 0.2 wt% Ti ion, are consistent with our Ti/Vycor sample giving O_2^-(III), except for the assistance of UV light in the present case.

The latter authors[30] observed the O_2^- stabilized on lower valence tungsten sites, such as W^{3+} or W^{4+} supported on SiO_2, which was almost identical to the present O_2^-(III). They simulated their temperature-dependent ESR line shapes between 77 and 418 °K using a rigid limit simulation program, the adjustable parameters being the apparent g value and orientation-dependent linewidth. Although the authors concluded that a temperature-dependent line shape of O_2^- on W/SiO_2 indicated anisotropic motion of O_2^- on the surface, detailed characterization of the surface motion of O_2^- requires simulation of the effects of slow motion, as they also noted.

3. O_2^-(III) prepared under UHV conditions and chemical reactivity with C_2H_4

When the Vycor supported Ti sample (aged sample) was prepared under UHV condition of $P \leq 10^{-9}$ Torr, a weak signal due to O_2^-(III) was observable after admission of 0.2 Torr O_2 at RT without UV irradiation. However, the signal did not grow significantly with further pressure of O_2. An intense signal of O_2^-(III) was formed by UV light and the sample was again evacuated to $P \leq 10^{-9}$ Torr and no difference in the temperature-dependent line shape of O_2^-(III) was observed between samples prepared and evacuated under a vacuum of 10^{-6} Torr and UHV conditions. These results indicate that the O_2^-(III) is strongly adsorbed on the Ti/Vycor surface, probably chemically bonded to Ti^{4+} on the surface, and, when the surface is prepared under UHV conditions, it does not affect the nature of the site or the molecular motion of surface O_2^-.

In order to examine the chemical reactivity of O_2^-(III), the C_2H_4 gases were introduced to the O_2^-(III) sample prepared under UHV conditions. Although no change on O_2^-(III) line shape was detected at RT after admission of $P \simeq 0.5$ Torr C_2H_4, when the sample was cooled below

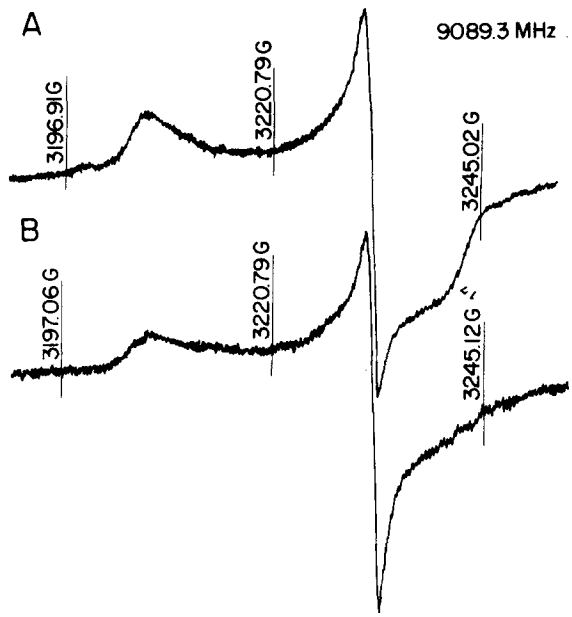

FIG. 4. ESR spectra suggesting interaction between O_2^-(III) and C_2H_4. Both spectra were recorded at 88 °K before (A) and after (B) 0.5 Torr C_2H_4 admission to the O_2^-(III) on Ti/Vycor. The Ti/Vycor sample giving the spectrum (A) was prepared under UHV conditions of 10^{-9} Torr and re-evacuation to 3×10^{-8} Torr after O_2^-(III) formation.

−140 °C, the spectrum showed a line shape different from the O_2^-(III) (cf. Fig. 4), which resembles an additional broadening of the outer regions of the spectrum. Upon warming the sample above −140 °C, the original spectrum of O_2^-(III) reappeared. However, when the O_2^-(III) sample was kept under 0.5 Torr C_2H_4 pressure at RT overnight, the O_2^-(III) signal almost completely decayed without giving any new ESR signal. The above results indicate that the O_2^-(III) might be weakly interacting with C_2H_4 at temperatures below about −140 °C but reacting with C_2H_4 slowly at RT.

4. ESR spectra of ^{17}O enriched O_2^-(III)

^{17}O enriched oxygen has proved to be a powerful tool in identifying the nature and the structure of oxygen species on oxides[23,31–33] and supported catalysis.[30,34–37] It has been reported that superoxide ions O_2^- have either equivalent[23,30–34] or nonequivalent oxygen nuclei[35–37] depending on the adsorbant. The O_2^- in the former case is believed to adsorb with the internuclear axis parallel to the surface and with the electron equally delocalized on the two oxygen nuclei. For the latter cases, a peroxy-type model (R–O–O^-) is suggested by several authors,[35–38] although the possibility of the O_2^- being adsorbed on a zig–zag surface leading to nonequivalent oxygen nuclei relative to the adsorption site[37] cannot be neglected.

Thus, an observation of ^{17}O hf splitting is really required in the present system in order to show that the spectrum is indeed due to a superoxide ion O_2^-, but not O^- and O_3^-, and to know if the O_2^- has either equivalent or nonequivalent oxygen nuclei. The experiments using ^{17}O enriched O_2 (70 at% of ^{17}O, 30 at% of ^{18}O) were carried out.

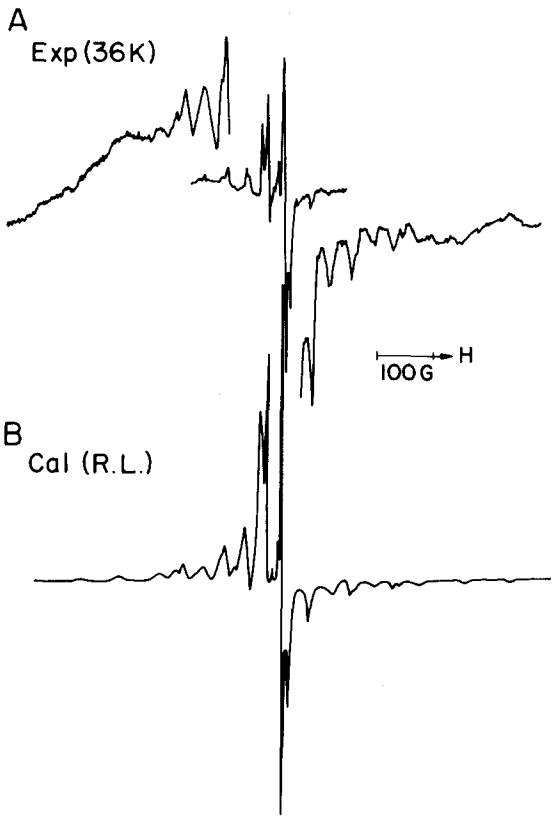

FIG. 5. Full spectra at 36 °K for ^{17}O enriched O_2^-(III). (a) Experimental spectrum. (B) Calculated spectrum by the rigid limit simulation program. Three different spectra $(^{17}O-^{18}O)^-$, $(^{17}O-^{17}O)^-$, and $(^{18}O-^{18}O)^-$ were superposed with relative intensities of 42:49:9. The parameters used for $(^{17}O-^{18}O)^-$ and $(^{17}O-^{17}O)^-$ were the same as those in Figs. 6(AII) and 6(BII). For $(^{18}O-^{18}O)^-$, the following parameters were used: $g_x=2.0027$, $g_y=2.0092$, $g_z=2.0267$, $1/T_{2x}^0=0.4$ G, $1/T_{2y}^0=0.2$ G, and $1/T_{2z}^0=0.5$ G.

An aged sample with 2 Torr $^{17}O_2$ was irradiated by UV light at 77 °K, warmed up to RT in order to remove thermally unstable paramagnetic species on the Vycor surface, and then evacuated to 10^{-6} Torr at RT. Then, the ESR spectra were recorded in the temperature range between 4.2 and 77 °K. The spectrum recorded at 36 °K is shown together with the simulated spectrum in Fig. 5. The spectra are completely different from those of $^{16}O_2^-$(III), since the complex spectra due to ^{17}O hfs of $(^{17}O-^{18}O)^-$ and $(^{17}O-^{17}O)^-$ are clearly visible. Thus, we can see that the molecular oxygen responsible for the spectrum, without doubt, does not come from the lattice oxygen of the Ti/Vycor, but from the oxygen added to the sample.

Since weak microwave power and modulation amplitude were employed in order to avoid line shape distrotion at low temperatures, especially at 4.2 °K, it was difficult to obtain a spectrum intense enough to determine the precise ESR parameters at 4.2 °K. Therefore, the spectrum at 36 °K was used to determine ESR parameters by means of ESR simulation using the rigid limit simulation program,[39] which includes second-order corrections.

In the expanded spectrum shown in Fig. 6, the resonance peaks corresponding to $(^{17}O-^{18}O)^-$, $(^{17}O-^{17}O)^-$, and $(^{18}O-^{18}O)^-$ are marked (*), (**), and (•), respectively. The best fit simulated spectrum to the $(^{17}O-^{18}O)^-$(*) is shown in Figs. 6(AII) and (AIII).

Based on our simulations, the following should be pointed out:

(1) The principal values of the ^{17}O hfs tensor were found to be almost axially symmetric with the perpendicular component $A_\perp(\simeq A_2\simeq A_3)$ being close to zero (or less than the linewidth of around 3 G).

(2) Two different parallel components of ^{17}O hfs were observed in $(^{17}O-^{18}O)^-$. They are $A_1(=A_\parallel)=74.8$ G and $A_1'(=A_\parallel)=80.3$ G and are clearly seen as a doublet at the $M_I=\pm\frac{5}{2}$ and $\pm\frac{3}{2}$ bands.

(3) The observed hf splittings of ^{17}O, i.e., A_1 and A_1', correspond to the g-tensor component of minimum value $g=2.0027$ at 36 °K.

(4) The relative peak heights of O_2^- having hf splittings A_1 and A_1' are not equal, but the former is apparently two times higher than the latter. Simulations were carried out based on two different assumptions. One is that the linewidth for each of the hf doublets is different, with that for A_1' being greater. The best fitting spectrum is shown in Fig. 6(AII). The other is that the intensity (or radical concentration) of the O_2^- giving A_1 is two times greater than that of A_1'. The spectrum simulated based on this assumption is shown in Fig. 6(AIII). Although one cannot see a big difference between the calculated spectra II and III, it seems that the spectrum II is in slightly better agreement with the observed one than is spectrum III.

Our observations (1) and (3) are consistent with those of previous workers (Refs. 23, 30–33, and 35–37). However, it should be noted that only in the present work have detailed spectral simulations been performed. It was found in our simulations that second-order hf corrections gave an important contribution to the spectrum. Two spectra were calculated using the rigid limit simulation program with and without second-order correction. A significant shift of the resonance positions was found in both cases. Therefore, to determine the precise ESR parameters the second-order contribution cannot be neglected. This contribution becomes more important in the $(^{17}O-^{17}O)^-$ spectrum as will be noted. Furthermore, it should be noted that the conclusions (2) and (3) are supported by the molecular orbital calculations using the extended Hückel method, the details of which will be discussed elsewhere.[40]

As mentioned already, the two different hyperfine splittings for $(^{17}O-^{18}O)^-$ have been discussed by several research groups.[35–37] Two explanations may be possible for this observation. One is that these two splittings refer to two oxygen nuclei in the same O_2^- ion, and the other arising from oxygen nuclei in two O_2^- ions in different surface sites. The observation of only one set of g values strongly suggests that the hf lines are from a single species. Furthermore, if two different species did exist in the system, it is probable that differences in

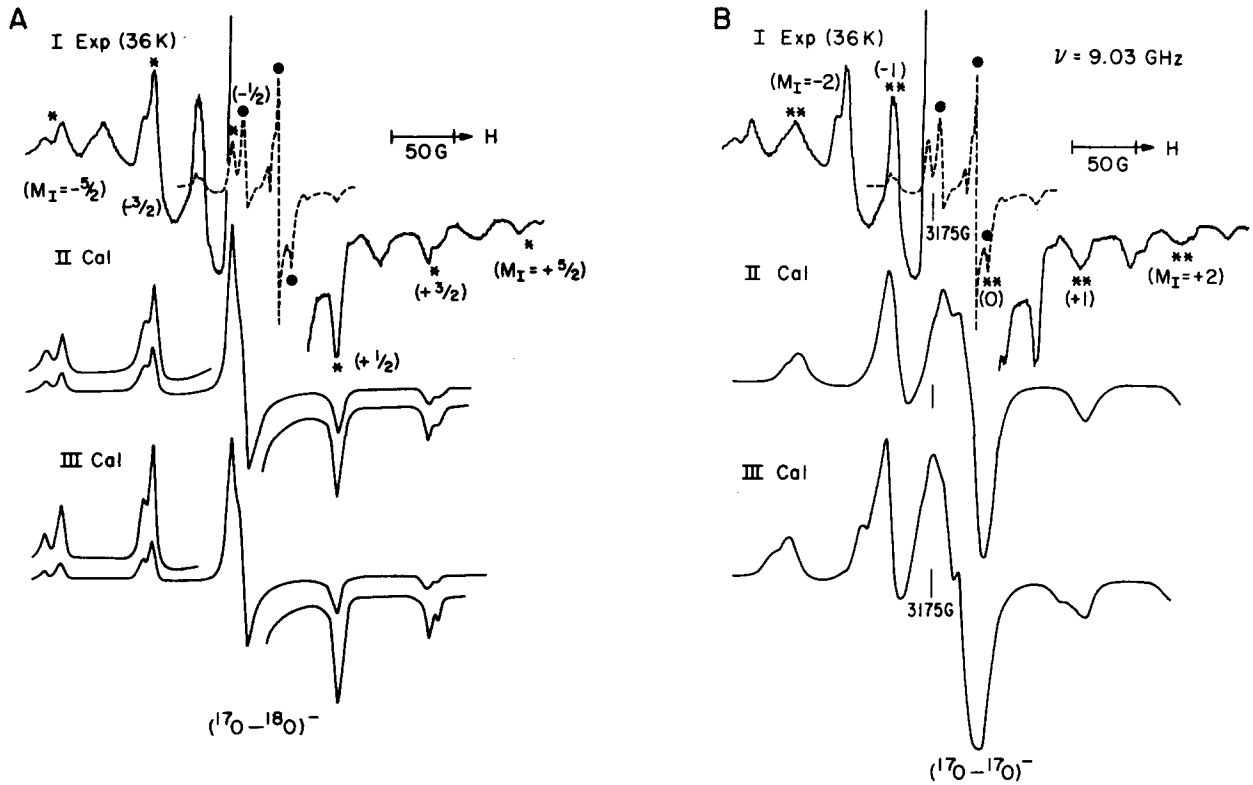

FIG. 6. Simulation of the $(^{17}O-^{18}O)^-$ (A) and the $(^{17}O-^{17}O)^-$ (B) spectra. (AI) and (BI): Experimental spectrum recorded at 36 °K. Expanded spectrum of the central part is shown. The bands marked as (*), (**), and (●) correspond to the $(^{17}O-^{18}O)^-$, $(^{17}O-^{17}O)^-$, and $(^{18}O-^{18}O)^-$, respectively. (AII), (BII) and (AIII), (BIII): Theoretical spectra calculated using the rigid limit simulation program (including the second-order correction) for two different sets of parameters:

	g_x	g_y	g_z	A_x (G)	A_y (G)	A_z (G)	$1/T_2^0$ (G)	Abundance (%)
II	2.0027	2.0092	2.0268	74.9	0	0	3	50
				80.3	0	0	5	50
III	2.0027	2.0092	2.0268	74.9	0	0	3	66.7
				80.3	0	0	3	33.3

Note that $1/T_2^0 = 6.0$ G was used for both (BII) and (BIII).

their relaxation times, rate of formation, or thermal stability would appear in the spectra. On the contrary, in the experiments using either $^{17}O_2$ or $^{16}O_2$, there were no such indications.

According to our simulation of the $(^{17}O-^{18}O)^-$ spectrum (using the rigid limit simulation program), two possibilities were suggested as noted in point (4). The latter one, viz., that the relative concentrations of O_2^- are different seems to be in contradiction with the model of two inequivalent nuclei in the same O_2^- because the probability of an ^{17}O occupying one of two oxygens in $(^{17}O-^{18}O)^-$ should be equal. Since we believe this model to be the case from the above arguments, we take the former possibility, viz., the widths of the A_1 and A_1' hf lines are different, probably due to a significant isotope effect on the motion of O_2^-, a possibility which could imply an important tunneling mechanism.[41]

Another way to potentially distinguish the two possibilities is to analyze the $(^{17}O-^{17}O)^-$ spectrum. The simulation of the $(^{17}O-^{17}O)^-$ spectrum was carried out for the two models, two nuclei in the same O_2^- but nonequivalent and two oxygen nuclei being equivalent but O_2^- present in two different sites with 1 : 2 ratio. The calculated spectra of II and III in Fig. 6(B) correspond to the former and the latter, respectively. The same ESR parameters were used as in the case of $(^{17}O-^{18}O)^-$. Unfortunately, we cannot see a clear difference between the calculated spectra based on the two different models because of a large linewdith of around 6 G being required in the simulation.

We now note that Che *et al.*[36,37] have proposed the following ways to distinguish the above two possibilities using the $(^{17}O-^{17}O)^-$ spectrum:

(1) In the case of the two oxygen nuclei being equivalent but O_2^- is in two different sites with the same g value, a series of doublets would be observed with a splitting $(A_1' - A_1)M_I$ providing that $|A_1 - A_1'| \ll A_1', A_1$, i.e., the separation of the doublets increases toward the extremities of the spectrum.

(2) In the case of the two nuclei in the same O_2^- being nonequivalent, the normally degenerate integer lines would be split into a number of components: a doublet for $M_I = \pm 4$, a triplet for $M_I = \pm 3$, etc.

(3) When the intrinsic linewidth is broader than the separation, then the resonance lines for the different M_I values should appear to be decreasing in width toward the center of the spectrum for the former case (i.e., two site model); on the other hand, they should be increasing for the latter case (i.e., single site model).

These arguments would be correct if the O_2^- were in the rigid limit and the two different hf splittings were small enough to neglect the second-order effect. On the contrary, in the observed spectra, the O_2^- is still affected by slow motion, and the line broadening due to the motion cannot be neglected. Furthermore, the hf splittings are in the 75–~80 G range for which the second-order contribution to the resonance position and the line shape cannot be neglected. In fact, the importance of the second-order term was clearly seen in the theoretical spectrum calculated for the two nonequivalent nuclei in the same O_2^- with and without the second-order term in the spin Hamiltonian.

In conclusion, although we could not unequivocally demonstrate that one of two possibilities was much better than the other, it seems to be reasonable to attribute the nonequivalent ^{17}O hfs to two nuclei in the same O_2^- being nonequivalent.

In this case the most probable model of the adsorption site should be of the peroxy radical type, i.e., one of two oxygen nuclei is more strongly bonded to the surface, probably to the Ti^{4+}, and the internuclei axis of O_2^- is no longer parallel to the surface. Molecular orbital calculations using the extended Hückel method[40] were carried out with the assumption that one of the two oxygens of O_2^- is located more closely to the Ti^{4+} and the angle of the internuclear axis is tilted from the parallel to the surface. According to the calculation, the spin density in the $2P_x$ orbital of the oxygen closer to Ti^{4+} was slightly less than that of the other oxygen (e.g., in the case of a 10° deviation, spin densities of 0.44 and 0.49 on $2P_x$ orbitals were estimated for the nonequivalent oxygens), the tendencies being consistent with the results on the ^{17}O hfs (the observed hf splittings of $A_{\|} = 74.8$ and 80.3 corresponding to the spin densities of 0.37 and 0.39, respectively[42]). Further details will be given elsewhere.[40]

Lastly, it should be noted that the line shape of $(^{18}O-^{18}O)^-$ at 36 °K [cf. Figs. 5(A) and 6(AI)] is considerably different from that of $(^{16}O-^{16}O)^-$ [cf. Fig. 2(A)], i.e., the degree of line broadening is much less for $(^{18}O-^{18}O)^-$ than for $(^{16}O-^{16}O)^-$. This significant isotope effect[43] on the motional dynamics, also, suggests the importance of a tunneling mechanism.[41]

C. Analysis of temperature-dependent spectra of $^{16}O_2^-$(III)

1. Determination of g-tensor components

In order to simulate slow motional spectra of $^{16}O_2^-$, one must know the components of the g tensor in the rigid limit. We have made our measurements on the O_2^-/Ti/Vycor sample in the manner given in the previous section. The lowest temperature of our measurements was 4.2 °K and the spectrum obtained is shown in Fig. 3(A). Although we believe that the spectrum at 4.2 °K is not the rigid limit, but has incipient slow motional effects, the g-tensor components should be very close to the rigid limit for the following reasons:

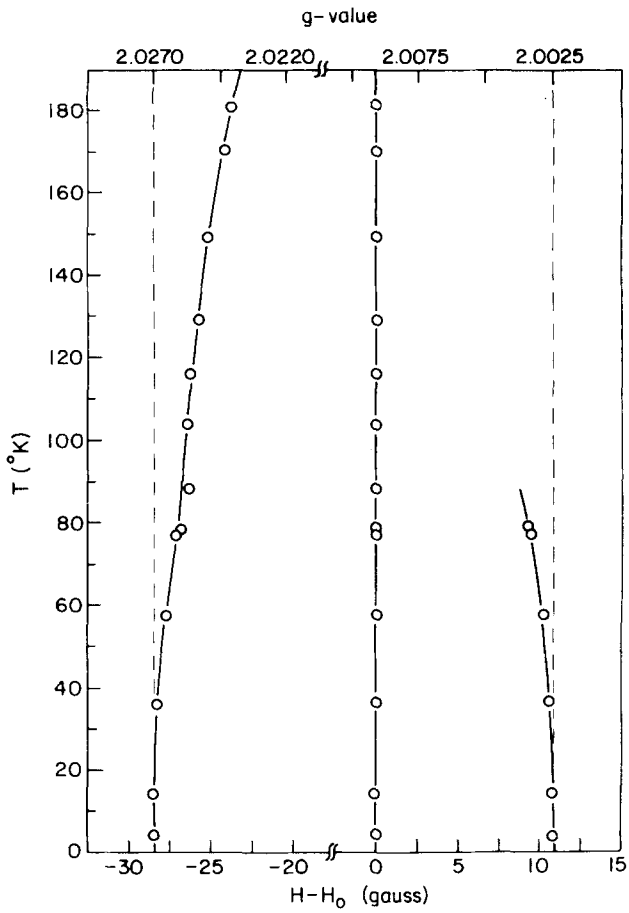

FIG. 7. Plot of experimental resonance positions vs temperature. H_0 stands for the magnetic field strength of 3221.06 G. Microwave frequency of $\nu = 9.058$ GHz was used.

(1) A variation of g components vs temperature is shown in Fig. 7. From this plot one can see that, below 14.5 °K, the components no longer change with temperature.

(2) The calculated spectrum using an orientation dependent linewidth and single linewidth are shown in Figs. 3(B) and 3(C). Although broader linewidths at both outer bands, which are believed to originate from residual motional effects, are required to simulate the observed spectrum using the rigid limit simulation program, shifts in the resonance positions should be negligible. The greater sensitivity of the linewidth (vs the shifts in position) to motional effects is analogous to the well known case in magnetic resonance and in nitroxide ESR spectra[44] where lines first broaden before they shift.

Thus, we will use the g-tensor components $g_1 = 2.0025$, $g_2 = 2.0092$, and $g_3 = 2.0271$ for $^{16}O_2^-$ at 4.2 °K as the rigid limit values in the following calculations.

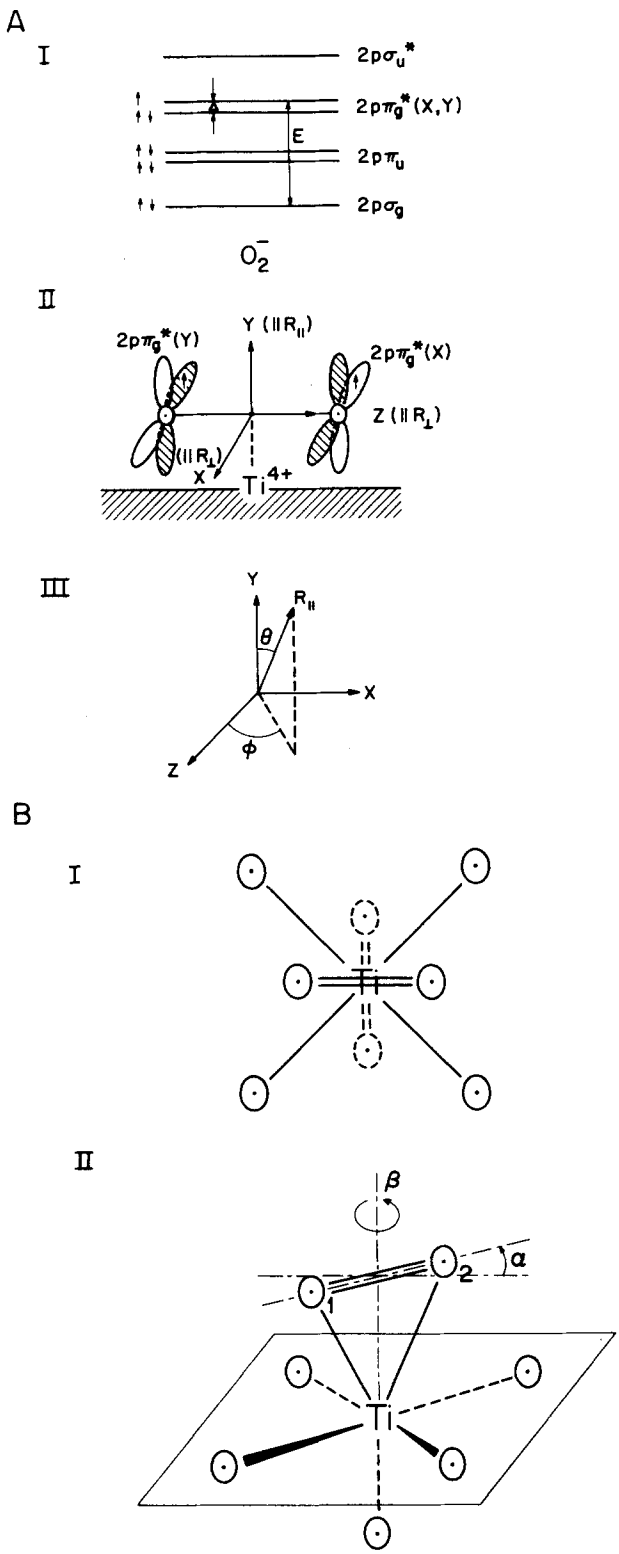

FIG. 8. (AI). Electronic energy levels of the superoxide ion O_2^-. (AII) Illustration of the molecular orbitals in which there is coincidence between the molecular coordinates and principal axes of the g tensor. In the slow motional calculations, the axis corresponding to R_{II} was chosen as parallel to y axis. (AIII) Illustration of the geometry showing the case in which the principal diffusion axis is not coincident with the principal axes of the O_2^- g tensor. (BI) Illustration of the geometry seen from the top, in which the C_{4v} symmetry is assumed for the Ti^{4+} site; moreover, the internuclear axis of O_2^- is assumed as parallel to the site. (BII) Illustration of the geometry used for the extended Hückel MO calculation (cf. Ref. 40).

2. *Temperature-dependent spectra of $^{16}O_2^-$(III)*

The observed spectra in the temperature region between 4.2 °K and room temperature are shown in Fig. 2. The following points should be noted for the spectra:

(1) The spectra are characterized by fully anisotropic g-tensor components and attributed to only one species of O_2^-. If several species did exist in the system, differences in thermal stability, rate of formation, or their relaxation times would appear in the spectra. On the contrary, none of these characteristics was detected by the experiments, as mentioned previously. Two independent groups[19,30] have reported nearly identical species of O_2^- (based on the g values and the temperature-dependent spectra) but in different systems, which tends to support the conclusion that the present spectra are attributable to only one species.

(2) The resonance position corresponding to $g_2 = 2.0092$ (center component of the g tensor) is independent of temperature below 200 °K, whereas the positions of the outer bands gradually shift to the center and broaden with increasing temperature, as shown in Figs. 2 and 7. This observation strongly suggests that the motion of O_2^- on the surface is anisotropic, in which the preferred axis of the motion is parallel to the direction of the center component of the g tensor ($g_2 = 2.0092$).

Studies on O_2^- have been extensively carried out for O_2^- trapped in a single crystal of alkali halides.[26,41,45–48] The g-value analysis by Känzig and Cohen[26] is well accepted and has been adapted by Kasai[49] and Lunsford[50] for this ion adsorbed on various oxides and supported catalysts. The electronic energy levels of adsorbed O_2^- in the ground state are schematically depicted as shown in Fig. 8(AI), the antibonding $2P\Pi g^*(x, y)$ orbital degeneracy of O_2^- is lifted by the crystal field Δ due to the Ti^{4+} ion where O_2^- is adsorbed. In this case, the principal values of the g tensor g_x, g_y, and g_z should be parallel to the molecular coordinates x, y, and z, as shown in Fig. 8(AII), where the ion on the surface is located on the y axis and the unpaired electron occupies the $2P\Pi g^*(x)$ orbital. g_z, the component along the internuclear axis, is expressed by $g_z \simeq g_e + 2\lambda/\Delta$, the value being shifted by $2\lambda/\Delta$ from g_e (the value for the free electron). Thus, the g_z component is very sensitive to the metal ion, as summarized by Lunsford[50] and Vedrine.[51] For the Ti^{4+}, the previously reported g_z values of O_2^-, i.e., between 2.03 and 2.02, are consistent with our present one. Furthermore, note that the small shift of g_x and g_y from g_e and $g_x < g_y$ are supported by the theory.[26,49] Thus, the present experimental values of g-tensor component can be reasonably correlated to the molecular form: $g_1 \equiv g_x = 2.0025$, $g_2 \equiv g_y = 2.0092$, and $g_3 \equiv g_z = 2.0271$.

The present ^{17}O experiments show that the ^{17}O hf tensor is axially symmetric and the parallel component splits at the g_x component of the g tensor. This result is consistent with the above argument that the unpaired electron occupies the $2P\Pi g^*(x)$ orbital, which is also consistent with the extended Hückel MO calculations.[40]

3. Spectral simulations

The spectral simulations of the temperature-dependent ESR spectra were carried out using the slow motional ESR simulation theory (programmed for a PDP-11 computer) for the different diffusion models[13]: Brownian diffusion, jump diffusion (from weak to strong jump), and approximate free diffusion.

Note that for anisotropic rotational diffusion, the eigenvalues $E_{L,K}$ of the diffusion operator are given by the expression

$$E_{L,K} = R_\perp B_L^\perp L(L+1) + (R_\parallel B_K^\parallel - R_\perp B_K^\perp) K^2 ,$$

where $B_L^\perp = [1 + R_\perp \tau_\perp L(L+1)]^{-P}$ and $B_K^\sigma = [1 + R_\sigma \tau_\sigma K^2]^{-P}$ ($\sigma = \parallel$ or $\perp$) and $P = 1$ for jump diffusion and $P = \frac{1}{2}$ for approximate free diffusion. The definitions of L, K, $\tau_\parallel$, and $\tau_\perp$ are given elsewhere,[13] but we note that the magnitude of $R_\perp \tau_\perp$ or $R_\parallel \tau_\parallel$ is a measure of the mean jump size (or approximate inertial effect). Simple Brownian diffusion is obtained by letting $R_\perp \tau_\perp$ and $R_\parallel \tau_\parallel \to 0$ so $B_L^\perp = B_K^\parallel = 1$. In the present paper, for the purposes of comparing different models, anisotropic rotational correlation times $\tau_{R_\parallel}$ and $\tau_{R_\perp}$ are defined as $\tau_{R_\parallel} \equiv (4R_\parallel B_2^\parallel)^{-1}$ and $\tau_{R_\perp} \equiv (6R_\perp B_2^\perp)^{-1}$. Furthermore, in order to study any line shape features due to the orientation of the main principal axis about which rotational diffusion occurs,[51] we varied the polar angles (θ and ϕ) [cf. Fig. 8(AIII)] which define the orientation of this axis relative to the coordinate system determined by the principal axes of the O_2^- g tensor. The importance of such nonzero "tilt" angles is suggested by the observation of nonequivalent ^{17}O hf splittings.

Before going into a comparison between the experimental and theoretical spectra, the sensitivity of the ESR line shape changes to slow molecular motion will be described for Brownian diffusion and weak jump diffusion.

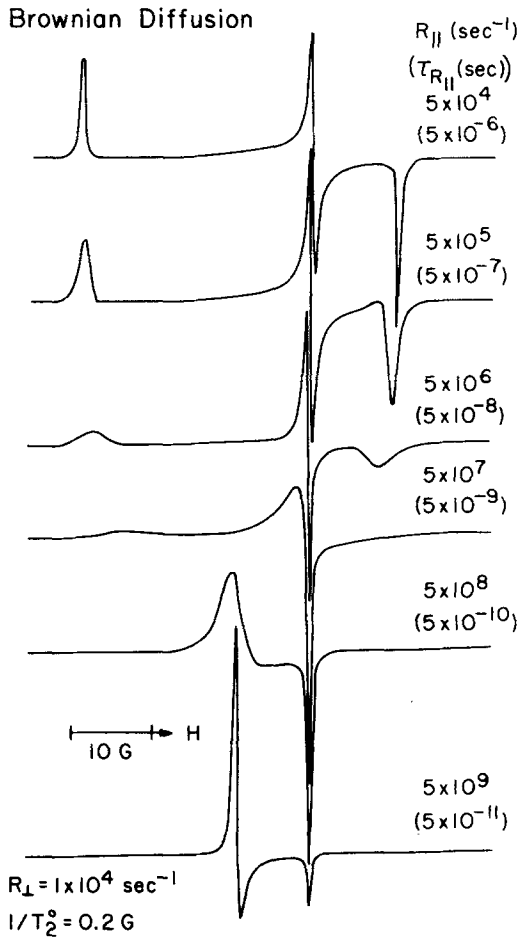

FIG. 9. Theoretical spectra illustrating the dependence in the line shape as a function of $R_\parallel$ (in units of sec^{-1}) for anisotropic Brownian diffusion. Here $g_x = 2.0025$, $g_y = 2.0092$, and $g_z = 2.0271$, which $R_\perp = 1 \times 10^4$ sec^{-1} the component of the diffusion tensor along the z axis, and a residual linewidth $1/T_2^0 = 0.2$ G.

4. Sensitivity of ESR spectra: Brownian diffusion and weak jump diffusion

Changes in the theoretical line shape of $^{16}O_2^-$(III) occurring as a function of $R_\parallel$ (in units of Sec^{-1}), the parallel component of the Brownian diffusion tensor, are shown in Fig. 9. They show the sensitivity of the ESR spectrum to molecular motion from $R_\parallel = 5 \times 10^4$ to 1×10^{10} sec^{-1}, i.e., from close to the rigid limit to the motionally narrowed region. For the calculation, axially symmetric Brownian diffusion along the axis perpendicular to the O–O internuclear axis (i.e., the y axis) was assumed [see Fig. 8(AII)]. (Note that for $R_\parallel \equiv R_y \gg R_x$, R_z, as is the case in our study, it follows that the anisotropic rotational diffusion can be treated rigorously as axially symmetric rotational diffusion with $2R_\perp \equiv R_x + R_z$.[52]) The g-tensor components used are those derived from the spectrum at 4.2 °K as discussed above. The value of $R_\perp$, the perpendicular component of the Brownian diffusion tensor, was chosen as 1×10^4 sec^{-1} ($N = R_\parallel / R_\perp = 5 - \sim 10^6$) and a residual linewidth of 0.2 G was used for the calculation. For $R_\parallel \leq 1 \times 10^5$ sec^{-1}, the line position of both outer bands (corresponding to the g_z and g_x components) were found to be essentially unshifted. Of course, the central position corresponding to g_y was unshifted with increasing $R_\parallel$ because of the model used for the calculation. However, the relative height of the central band to the outer bands becomes greater with increasing $R_\parallel$, because the latter are broader.

The theoretical spectrum calculated for $R_\parallel = 5 \times 10^4$ sec^{-1} and $R_\perp = 1 \times 10^4$ sec^{-1} (i.e., $\tau_{R_\parallel} = 5 \times 10^{-6}$ sec, $\tau_{R_\perp} = 1.7 \times 10^{-5}$ sec) corresponds well to both the line shape and the line positions of the spectrum calculated by the rigid limit simulation. Thus, for rotational correlation times longer than the above values, no detectable changes on the ESR line shape are to be expected.

In the slow motional region between $R_\parallel = 5 \times 10^5$ and 1×10^7 sec^{-1} ($\tau_{R_\parallel} = 5 \times 10^{-7}$ sec and $\tau_{R_\parallel} = 2.5 \times 10^{-8}$ sec, $N = 50 - \sim 10^3$), the outer band positions are gradually shifted inward with increasing $R_\parallel$, while drastic line broadening is seen on the outer bands. In the intermediate region of rotational diffusion motion between $R_\parallel = 5 \times 10^7$ and 1×10^8 sec^{-1} [$\tau_{R_\parallel} = (5 - \sim 2.5) \times 10^{-9}$ sec, $N = 5 \times 10^3 - \sim 10^4$], the outer bands almost disappear because of line broadening, and an asymmetric singlet centered at g_y is observed. In the motional narrowing region of $R_\parallel \geq 5 \times 10^8$ sec^{-1} ($\tau_{R_\parallel} \leq 5 \times 10^{-10}$ sec, $N \geq 5 \times 10^4$), a new band ap-

pears at $g = \frac{1}{2}(g_x + g_z)$ position, the band becoming gradually narrower with $R_{\parallel}$. When the experimental spectra are compared with the theoretical ones, the rotational diffusion motion of O_2^- will be found to be in the slow motional region for $R_{\parallel} \leq 5\times10^7$ sec^{-1} ($\tau_{R_{\parallel}} \geq 5\times10^{-9}$ sec) based on the Brownian diffusion model. The more detailed discussion will be given later.

Next, the contribution of $R_{\perp}$ to the line shape for the Brownian diffusion model is considered. The theoretical spectra were calculated as a function of $R_{\perp}$. The typical value of a slow motional $R_{\parallel} = 1\times10^6$ sec^{-1} was used for the calculation, while $R_{\perp}$ was varied in the range from $R_{\perp} = 1\times10^3$ sec^{-1} to $R_{\perp} = 5\times10^5$ sec^{-1} for the same g-tensor components as in the case of Fig. 9. In the region between $R_{\perp} = 1\times10^3$ sec^{-1} and $R_{\perp} = 1\times10^4$ sec^{-1} [$\tau_{R_{\parallel}} = 2.5\times10^{-7}$ sec for $N = 10^3 - \sim 10^2$ or $\tau_{\bar{R}} = (1.7 - \sim 5.3)\times10^{-6}$ sec], no change in the line shape is seen. Thus, one can say that the contribution of $R_{\perp}$ to the line shape is negligible when a value of $R_{\perp} \leq 1\times10^4$ sec^{-1} is used for the calculation. In the region between $R_{\perp} = 1\times10^4$ and 5×10^4 sec^{-1}, one can see the peak height of the outer bands become stronger with respect to that of the central band, but the line positions remain constant. Above $R_{\perp} \geq 5\times10^5$ sec^{-1} ($\tau_{\bar{R}} \leq 2.4\times10^{-7}$; $N \geq 2$), the line positions start to shift to the center. Another interesting observation is that the apparent linewidths at both outer bands are essentially independent of the values of $R_{\perp}$ between 1×10^3 and 5×10^5 sec^{-1}, whereas significant broadening of the central band occurs above $R_{\perp} = 1\times10^4$ sec^{-1}. [Note $\bar{R} \equiv \sqrt{R_{\parallel} R_{\perp}}$ and $\tau_{\bar{R}} \equiv (6\bar{R})^{-1}$].[13]

Another important parameter affecting the predicted line shapes of slow motional ESR spectra is the residual linewidth $1/T_2^0$. In order to see the sensitivity of the slow motional spectra for anisotropic Brownian diffusion to $1/T_2^0$, theoretical spectra were calculated as a function of $1/T_2^0$ for the typical values of $R_{\parallel} = 5\times10^6$ sec^{-1} and $R_{\perp} = 5\times10^3$ sec^{-1} ($\tau_{R_{\parallel}} = 5\times10^{-8}$ sec, $N = 10^3$). Although no shift of line position is seen, as expected the line shape changes significantly with a small variation of $1/T_2^0$ from 0 to 0.75 G. Thus, one has to be very careful of a proper choice of $1/T_2^0$ in simulating the experimental spectrum. Our way of finding a satisfactory linewidth will be discussed in the section on jump diffusion.

We also tested the sensitivity of slow motional ESR spectra by using the weak jump diffusion model with $R_{\parallel}\tau_{\parallel} = 0.1$, $R_{\parallel}$ and $\tau_{\parallel}$ being rate of diffusion along y axis and mean jump time, respectively. The changes of line shape in the slow motional region from $R_{\parallel} = 1\times10^6$ to 2×10^7 sec^{-1} [$\tau_{R_{\parallel}} = (3.5\times10^{-7}) - (1.8\times10^{-8})$ sec, $N = 10^2 - \sim 10^3$] are illustrated in Fig. 10. The important point seen from the theoretical spectra is that linewidths of the outer bands for jump diffusion are much broader than for Brownian diffusion for the spectra giving the same line position. As shown in the spectra for $R_{\parallel} \leq 2\times10^6$ sec^{-1} ($\tau_{R_{\parallel}} \geq 1.8\times10^{-7}$ sec; $N \leq 2\times10^2$), the outer line positions of the near rigid limit spectra do not shift from those of the completely rigid limit; however, strong line broadening is seen at the outer bands. Thus, the greater sensitivity of the linewidth vs the shift in position can be clearly demonstrated for weak jump diffusion.

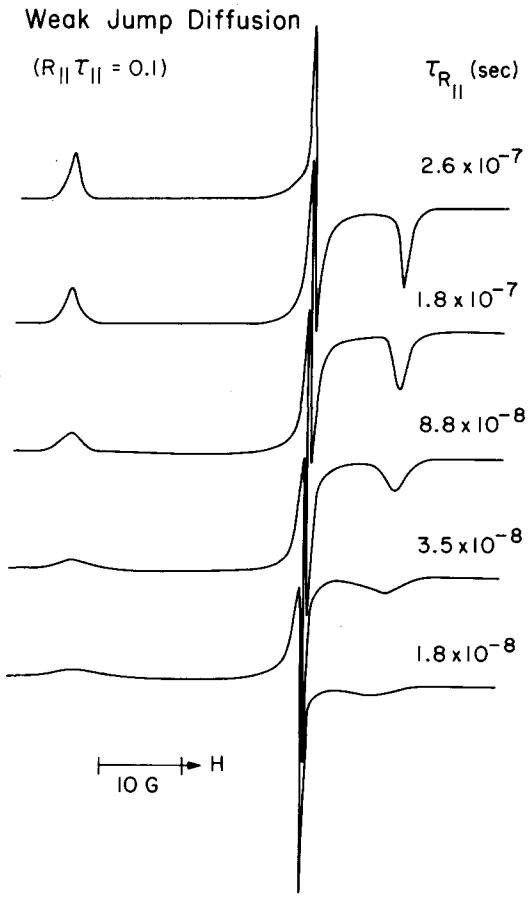

FIG. 10. Theoretical spectra illustrating the change in the line shape occurring as a function of $R_{\parallel}$ (or $\tau_{\parallel}$) of anisotropic weak jump diffusion ($R_{\parallel}\tau_{\perp} = 0.1$), for $g_x = 2.0025$, $g_y = 2.0092$, $g_z = 2.0271$, $R_{\perp} = 1\times10^4$ sec^{-1}, and $1/T_2^0 = 0.2$ G. $R_{\parallel}$ and $\tau_{\parallel}$ are the rate of diffusion along the y axis and the mean jump time, respectively.

5. *Comparison between experimental and theoretical spectra*

The simulated and experimental spectra (below 80 °K) are compared in Figs. 11(A), 11(B), and 11(C) for the different models and different temperatures. Since the theoretical spectra calculated for weak jump diffusion seems to best fit the experimental spectra below 80 °K, as seen from the figures, we first discuss the case of jump diffusion.

Jump diffusion: For jump diffusion from weak jump ($R_{\parallel}\tau_{\parallel} \sim 0.1$) to strong jump ($R_{\parallel}\tau_{\parallel} \sim 10$), the simulation was carried out using as variable parameters $R_{\parallel}$, $\tau_{\parallel}$, and $1/T_2^0$ and as fixed parameters $R_{\perp} = 1\times10^4$ sec^{-1}, $\tau_{\perp} = 0$.

In Fig. 12, the importance of a proper choice of $1/T_2^0$ is illustrated. The simulation was carried out for the experimental spectrum recorded at 36 °K using a weak jump diffusion model ($R_{\parallel}\tau_{\parallel} = 0.1$). It is clearly seen from the figure that a small variation of $1/T_2^0$ from 0.1 to 0.3 G results in a considerable change in line shape of theoretical spectrum, especially on the outer band peak heights (corresponding to g_x and g_z) with respect to the central band at g_y. In the present studies, the linewidth $1/T_2^0$ giving the same spectral peak heights as

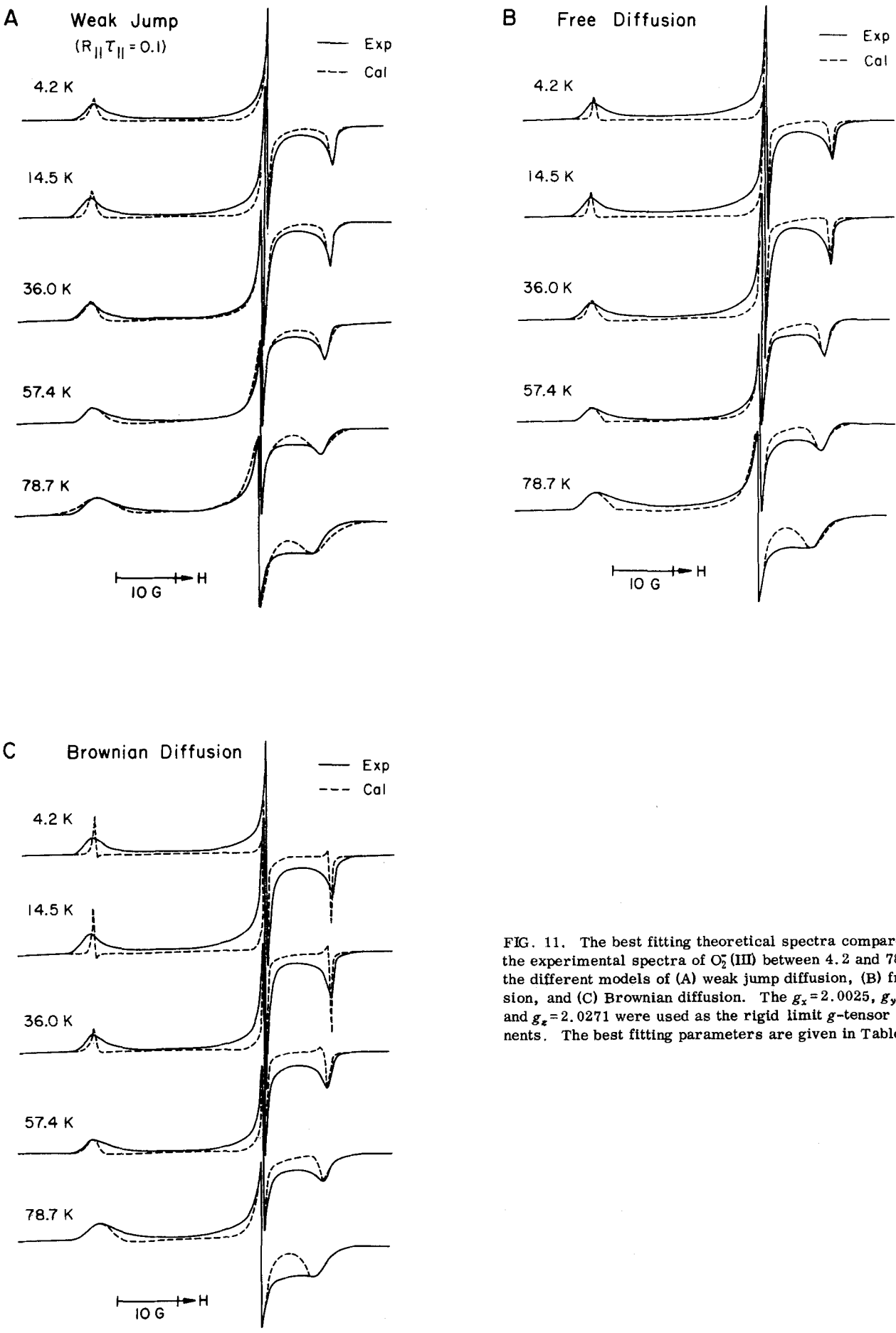

FIG. 11. The best fitting theoretical spectra compared with the experimental spectra of O_2^-(III) between 4.2 and 78.7°K for the different models of (A) weak jump diffusion, (B) free diffusion, and (C) Brownian diffusion. The $g_x = 2.0025$, $g_y = 2.0092$, and $g_z = 2.0271$ were used as the rigid limit g-tensor components. The best fitting parameters are given in Table III.

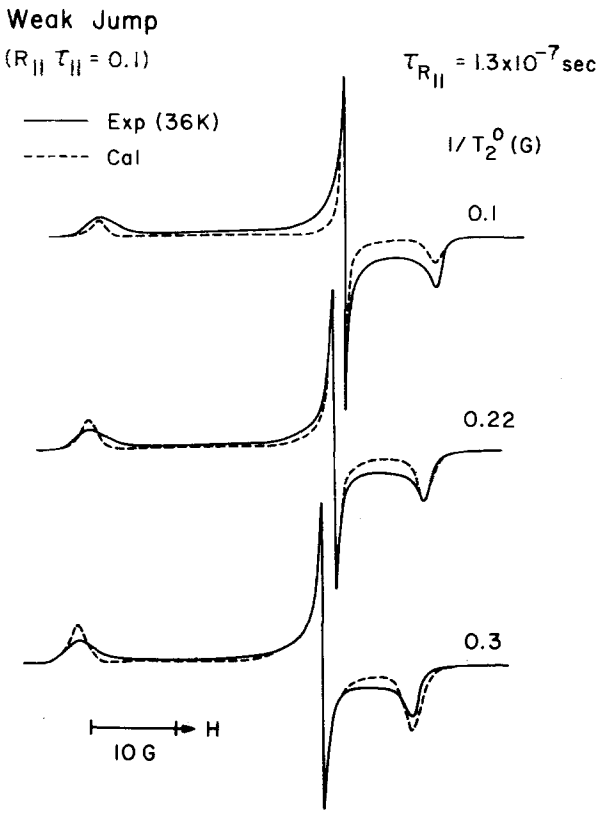

FIG. 12. Theoretical spectra illustrating the sensitivity of slow motional spectra (corresponding to the experimental spectrum at 36 °K) of anisotropic weak jump diffusion ($R_{||}\tau_{||} = 0.1$) to the linewidth $1/T_2^0$, for $R_{||} = 2.7\times10^6$ sec^{-1}, $\tau_{||} = 3.7\times10^{-8}$ sec, $R_\perp = 1\times10^4$ sec^{-1}, $g_x = 2.0025$, $g_y = 2.0092$, and $g_z = 2.0271$.

those of the central band (g_y) and high field band (g_x) was taken as a good linewidth, e.g., $1/T_2^0 = 0.22$ G is a good linewidth for the spectrum at 36 °K, as seen in the figure.

The simulation of the experimental spectrum at 36 °K was carried out as a function of $R_{||}\tau_{||}$, with $R_{||}\tau_{||}$ being varied from 0.1 to 10. Here $R_{||}$ (sec^{-1}) was chosen as the variable parameter, a constant value of $\tau_{||}$ (3.8×10^{-8} sec) being used for this case. The theoretical spectra are compared with the experimental one. With increasing value of $R_{||}\tau_{||}$, a broader linewidth was needed to fit both intensities of the central and high field bands. Although the coincidence of line position is quite good for the experimental vs theoretical spectra, that of the line shape becomes gradually worse with $R_{||}\tau_{||}$. Thus, a weak jump model is the best among the jump diffusion models.

As seen in Fig. 11(A), the theoretical spectra calculated using the weak jump diffusion model ($R_{||}\tau_{||} = 0.1$) are fairly close to a series of experimental spectra, especially below 57 °K. This gives us some confidence that our approach for analyzing the spectra is reasonable. However, with increasing temperature, i.e., increasing rate of diffusion, the agreement between theoretical and experimental spectra becomes gradually worse as shown in Fig. 13. No improvement in the line shape is seen by changing value of $R_{||}\tau_{||}$. In the same figure the theoretical spectra calculated using a strong jump model ($R_{||}\tau_{||} = 10$) are also illustrated (see the spectra corresponding to 149 and 181 °K).

Brownian diffusion and approximate free diffusion: The simulated spectra using approximate free diffusion and Brownian diffusion are compared with observed spectra below 80 °K in Figs. 11(B) and 11(C). Although the calculated spectra are in reasonable agreement with the observed ones at 57.4 and 78.7 °K, the agreement between observed and calculated spectra becomes worse with decreasing temperature (i.e., increasing $\tau_{R_{||}}$) in the incipient slow motional region, especially for the Brownian diffusion model.

We note the following based on the present simulations:

(1) The degree of line broadening for the outer bands is much less for Brownian diffusion than for weak jump diffusion when both models yield the same outer line positions, especially in the incipient slow motional region.

(2) In accord with (1), to get the same degree of line broadening the Brownian diffusion model requires a larger shift of line position than does the weak jump model.

(3) Moreover, in order to simulate the spectrum at a given temperature, a larger correlation time $\tau_{R_{||}}$ is needed for Brownian diffusion than for weak jump. For example, from the best fit simulation of line positions at 36 °K, the $\tau_{R_{||}} = 1\times10^{-6}$ sec and $\tau_{R_{||}} = 1.3\times10^{-7}$ sec were obtained for Brownian and weak jump diffusion models, respectively (cf. Table III and Fig. 11).

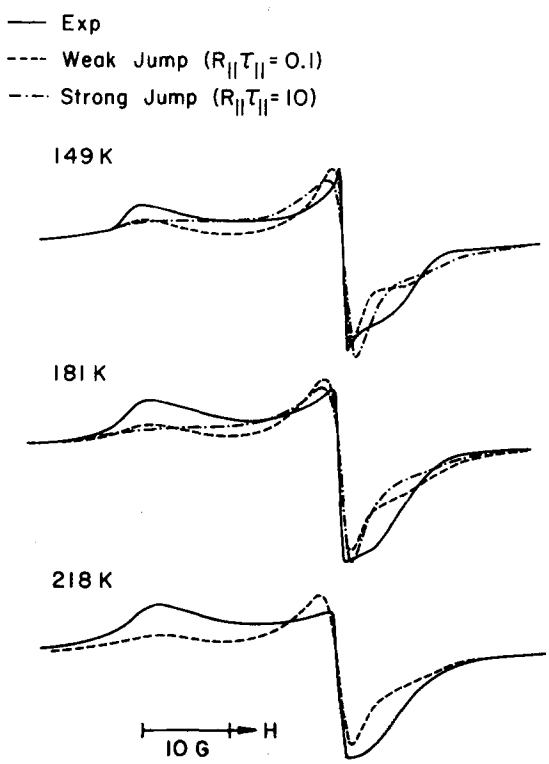

FIG. 13. Experimental spectra between 149 and 218°K compared with the theoretical ones for the weak jump diffusion ($R_{||}\tau_{||} = 0.1$) and strong jump diffusion. The parameters used for $R_{||}$, $\tau_{||}$, and $R_\perp$ are given in Table III. $1/T_2^0 = 2.0$ G was used.

TABLE III. Best fitting parameters of slow motional ESR spectra.

T (°K)		$R_{\parallel}$ (sec^{-1})	$\tau_{\parallel}$ (sec)	$\tau_{R_{\parallel}}$ (sec)	$1/T_2^0$ (G)
4.2 °K (14.5 °K)	B.D.[a]	1.0×10^{4}	···	2.5×10^{-5} ($N\geqslant1$)	0.00
	J.D.[a]	1.1×10^{6}	8.8×10^{-8}	3.2×10^{-7} ($N\geqslant1.1\times10^{2}$)	0.1
	F.D.[c]	2.0×10^{5}	5.0×10^{-7}	1.4×10^{-6}	0.01
36.0 °K	B.D.	2.5×10^{5}	···	1.0×10^{-6} ($N\geqslant25$)	0.03
	J.D.	2.7×10^{6}	3.8×10^{-8}	1.3×10^{-7} ($N\geqslant2.7\times10^{2}$)	0.22
	F.D.	1.1×10^{6}	0.88×10^{-8}	2.5×10^{-7} ($N\geqslant1.1\times10^{2}$)	0.12
57.4 °K	B.D.	1.0×10^{6}	···	2.5×10^{-7} ($N\geqslant10^{2}$)	0.12
	J.D.	6.7×10^{6}	1.5×10^{-8}	5.2×10^{-8} ($N\geqslant6.7\times10^{2}$)	0.45
	F.D.	2.7×10^{6}	3.8×10^{-8}	9.9×10^{-8} ($N\geqslant2.7\times10^{2}$)	0.23
78.7 °K	B.D.	5.0×10^{6}	···	5.0×10^{-8} ($N\geqslant5\times10^{2}$)	0.45
	J.D.	1.3×10^{7}	7.5×10^{-9}	2.7×10^{-8} ($N\geqslant1.3\times10^{2}$)	0.80
	F.D.	6.7×10^{6}	1.5×10^{-8}	4.1×10^{-8} ($N\geqslant6.7\times10^{2}$)	0.55
104 °K	B.D.	7.0×10^{6}	···	3.8×10^{-8}	
	F.D.	1.0×10^{7}	1.0×10^{-8}	3.0×10^{-8}	
129 °K	B.D.	1.0×10^{7}	···	2.5×10^{-8}	
149 °K	B.D.	2.0×10^{7}	···	1.3×10^{-8}	
	J.D.	2.5×10^{7}	4.0×10^{-9}	1.4×10^{-8}	
	F.D.	2.0×10^{7}	5.0×10^{-9}	1.5×10^{-8}	
181 °K	J.D.	4.0×10^{7}	2.5×10^{-9}	8.8×10^{-9}	
	F.D.	3.0×10^{7}	3.3×10^{-9}	1.0×10^{-8}	
218 °K	J.D.	5.0×10^{7}	2.0×10^{-9}	7.0×10^{-9}	
	F.D.	4.0×10^{7}	2.5×10^{-9}	7.5×10^{-9}	
263 °K	B.D.	4.0×10^{7}	···	6.3×10^{-9}	

[a]B. D. = Brownian diffusion.
[b]J. D. = jump diffusion.
[c]F. D. = free diffusion.

(4) Approximate free diffusion was found to be intermediate between Brownian and weak jump diffusions with respect to the above three points.

Thus, it is concluded that the jump model is able to yield the best fit to the observed spectra in the lower temperature region below 57.4 °K.

However, a Brownian diffusion model seems the best above this temperature among the models used, although the spectra are not simulated very satisfactorily. In Fig. 14, the theoretical spectra calculated on the basis of the Brownian diffusion model are shown and compared with the observed spectra in the higher temperature region.

Simulation of spectra in the higher temperature region: Although the line shapes cannot be reproduced satisfactorily, the correlation time $\tau_{R_{\parallel}}$ is estimated in this higher temperature range from the theoretical spectra which give the same line position as the observed ones. The values of $\tau_{R_{\parallel}}$ obtained for the three different models are plotted vs $1/T$ (°K^{-1}) in Fig. 15, together with those estimated in the lower temperature region. From this plot, one can see that $\tau_{R_{\parallel}}$ is essentially independent of the model used above 100 °K and decreases exponentially vs $1/T$ (°K^{-1}), whereas in the very slow motional region, the $\tau_{R_{\parallel}}$ depends strongly on the model and is no longer simply exponential with $1/T$ (°K^{-1}). (The temperature independent $\tau_{R_{\parallel}}$ below 14.5 °K will be discussed below in terms of quantum mechanical motion.) The activation energy of 0.5 kcal/mole was evaluated for the rotational diffusion of O_2^- from the linear relation between ln $\tau_{R_{\parallel}}$ and $1/T$ above 100 °K. The small activation energy for the rotational motion will be discussed below.

We now turn to the features of the line shape in the higher temperature region. Two characteristics of the observed line shape are the linewidth broadening and asymmetry of the central band (cf. the experimental spectra above 180 °K) and the line position (corresponding to g_y) which is also beginning to shift above 200 °K. These trends can be partially reproduced by increasing $R_{\perp}$ (sec^{-1}) as shown in Fig. 16, although the result is far from a successful agreement with observed line shape. (Note that the effect of increasing $R_{\perp}$ appears in the line broadening at the central band and the line position shifting due to mixing g_y and g_z and g_y and g_x components.)

We recall that our analysis is based on a model of axially symmetric motion such that $R_{\parallel}\gg R_{\perp}$.[52] The nature

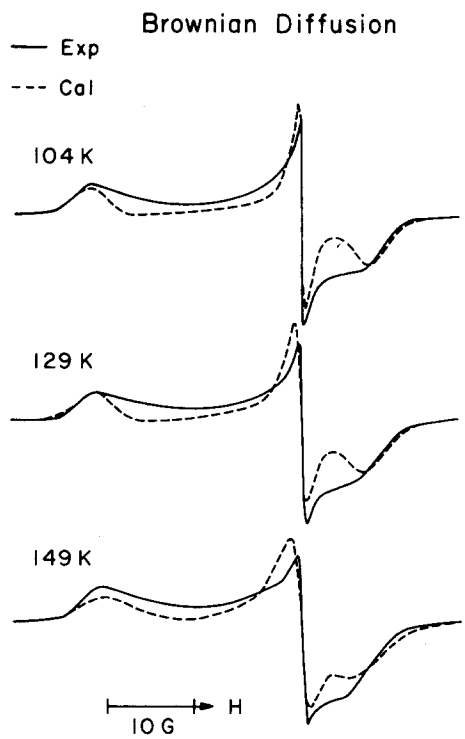

FIG. 14. Experimental spectra between 104 and 149 °K compared with the theoretical ones for Brownian diffusion. The spectra were calculated using parameters $R_{\parallel}$ and $R_{\perp}$ given in Table III. The linewidths $1/T_2^0=0.7$, 0.9, and 1.5 G were used for the spectra corresponding to 104, 129 and 149 °K, respectively.

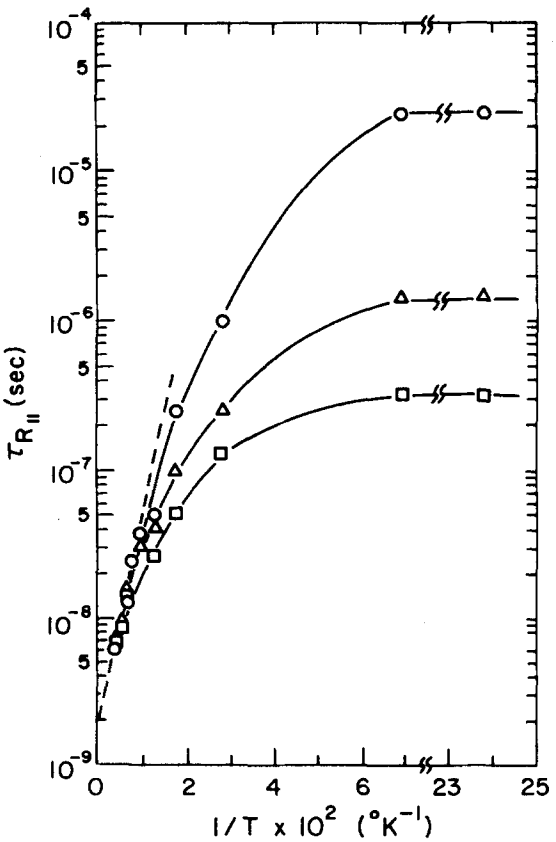

FIG. 15. Plot of $\tau_{R\parallel}$ vs $1/T$ using the data in Table III. The analysis based upon Brownian diffusion is given by ⊙, that for free diffusion ($R_{\parallel}\tau_{\parallel}=0.1$) by △, and that for jump diffusion ($R_{\parallel}\tau_{\parallel}=0.1$) by ⊡.

of the site of the O_2^-/Ti^{4+} complex [cf. Fig. 8] suggests, however, that there should not be any axial symmetry to the motion. In general, we expect $R_{\parallel} \equiv R_y \gg R_x$, R_z, but one might further expect that $R_x \gg R_z$, since a nonzero R_z would imply rotating the Ti^{4+} complex embedded on the surface. We have already noted that for $R_{\parallel} \gg R_x$, R_z, the rotational diffusion equations are well approximated by $R_{\perp} \equiv \frac{1}{2}(R_x + R_z)$ even if $R_z = 0$ [i.e., any rotation about the z axis can be equivalently performed by a sequence of (1) a fast rotation about the y axis; (2) a slow rotation about the x axis; and (3) another fast rotation about the y axis]. However, the spectral asymmetry is consistent with a higher rate of averaging between g_y and g_z (e.g., by rotations about the x axis) than that between g_y and g_x (e.g., by rotations about the z axis). We shall next discuss the spectral effects of a tilt of the O_2^- relative to the surface plane and by only $R_{\parallel}$ nonzero. However, it could be that as the O_2^- rotates about the y axis, there is a "wobble" of the O_2^- about the x axis. Such a possibility would be consistent with our extended Hückel calculations[40]; it would be consistent with the spectral asymmetry; and it would imply incomplete averaging about the x axis, for which it would no longer be true that we could employ a simple $R_{\perp} \equiv \frac{1}{2}(R_x + R_z)$.

Effects of tilt of axes: In the experiments using ^{17}O, nonequivalent oxygen nuclei were detected for $^{17}O_2^-$. Two possibilities were suggested for the origin of nonequivalent oxygen nuclei. One is two oxygen nuclei in the same O_2^- ion with different hfs (the other being oxygen nuclei in two O_2^- in different surface sites). If the former is the case (which we believe), the internuclear axis of O_2^- is no longer parallel to the surface. Therefore, in order to see how the line shape changes with the orientation of axis about which the motion occurs,[52] we calculated the theoretical spectra as a function of the polar and azimuthal angles (θ and ϕ) between the orientation of the diffusion axis and the principal coordination system of g tensor [see Fig. 8(AIII)]. It is found that the theoretical spectra are not sensitive to tilt for $\theta \leq 10^\circ$ and $\phi \leq 10^\circ$, but for $\theta > 10^\circ$ and $\phi > 10^\circ$ the line shapes change and the line positions are gradually shifted. As one example, the theoretical spectra (corresponding to the experimental spectrum at 129 °K) of anisotropic Brownian diffusion are illustrated in Fig. 17 in order to show the sensitivity of line shape changes as a function of θ. It is seen from the spectra that (1) with increasing θ, the positions of the central and high field lines are shifted to the higher field side; on the other hand, that of the low field line is moved to the lower field side with respect to the position at $\theta = 0$; (2) at the same time, the linewidth becomes broader at the central band and the peak heights increase at the outer bands.

However, the trends are found to be worsening the agreement between the experimental and theoretical spectra. Furthermore, it is found that neither the

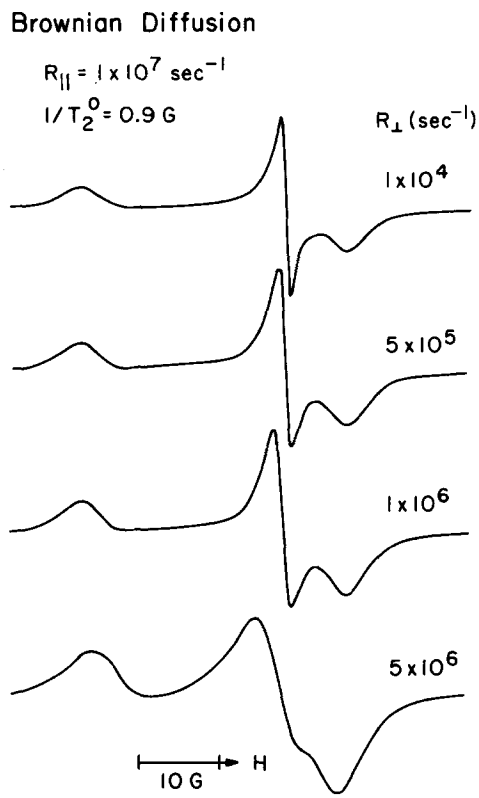

FIG. 16. Theoretical spectra illustrating the change in the line shape occurring as a function of $R_{\perp}$ for anisotropic Brownian diffusion. The spectrum for $R_{\perp} = 1 \times 10^4$ sec^{-1} corresponds to the experimental one at 129°K.

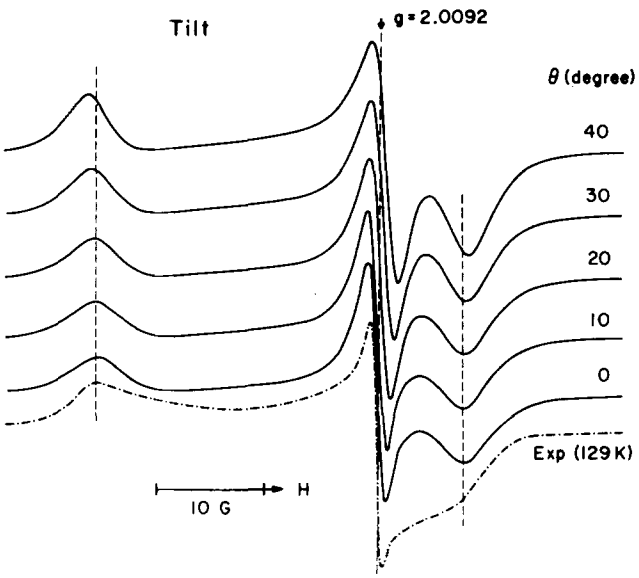

FIG. 17. Theoretical spectra (corresponding to the experimental spectrum at 129 °K for $\theta = 0°$) illustrating the change in the lineshape occurring as a function of tilt angle θ of the anisotropic Brownian model for $R_{\parallel} = 1.0 \times 10^7$ sec^{-1}, $R_{\perp} = 1 \times 10^4$ sec^{-1}, and $1/T_2^0 = 0.9$ G.

other models nor the addition of the angle ϕ improves the line shapes. Therefore, it appears that, even if the diffusion axes and the principal axes are not coincident, the angle(s) should be small, probably less than 10°.

We note that this discussion refers to a model of constant tilt, but not to the wobble model suggested in the previous section, in which the mean tilt angle could still be small.

Discrete jump model: The discrete jump model is also of interest, because there is a possibility of O_2^- jumping between several discrete sites corresponding to large potential energy minima on the surface [cf. Fig. 8(BI)] as is seen in several systems.[17,53]

The theoretical spectra were calculated for in-plane $\pi/2$ jumps about the normal to internuclear axis of O_2^- [see Fig. 8(BI)] in which g_y remained invariant but g_x and g_z switched positions. The calculated spectra are shown in Fig. 18 as a function of τ_j, mean life time between jumps. Characteristics derived from the spectra are summarized as follows:

(1) The band, which becomes predominant in a fast jump process, appears at $g = (g_x + g_z)/2$ position even in a region of slow jump ($\tau_j \geq 10^{-8}$ sec).

(2) The symmetry of the central band, which is characteristic of experimental spectra in the low temperature region, is destroyed.

(3) The sensitivity of the linewidth broadening vs shifts in line position is much greater than in any other models used in the present studies. For example, although for $\tau_j \geq 10^{-8}$ sec a considerable line broadening is seen at outer bands, the positions are not shifted essentially from the rigid limit.

Although the peak height of the extra band decreases gradually with increasing τ_j, the series of experimental spectra cannot be analyzed by this discrete in-plane $\pi/2$ jump model because of the existence of the extra band in the theoretical spectra.

Theoretical spectra were also calculated for in-plane $2\pi/3$ jumps. Similar to the case for the $\pi/2$ jumps, the extra band appears at $g = 3(g_x + g_z)/4$ even in a region of slow jumping, again inconsistent with experiment.

6. Discussion of quantum effects on the motions

Free planar motion: First we note that the characteristic rotational temperature for O_2^- is $\theta_r \equiv \hbar^2/2Ik = 2.07$ °K, which is not small near 4 °K. If we assume completely free planar rotation, then the allowed rotational states for the Bose system $^{16}O-^{16}O^-$ are

$$\psi_m = \frac{1}{\sqrt{2\pi}} e^{im\phi}, \quad m = 0, \pm 2, \pm 4, \ldots, \tag{1a}$$

with eigenvalues

$$E_m = m^2 \hbar^2/2I. \tag{1b}$$

In the limit where the O_2^- rotor is only weakly affected by thermal modes, we can assume an ensemble of rotors distributed according to a Boltzmann distribution but can neglect transitions among the rotational states in computing the ESR line shapes.

The spin Hamiltonian in the secular (high-field) approximation is

$$\begin{aligned} \mathcal{H}_0 &= g_{av} \hbar^{-1} \beta_0 \mathcal{B}_0 S_z, \\ \mathcal{H}_1(\theta, \phi) &= \mathcal{F}_0 \mathcal{D}^2_{0,0}(\phi, \theta, 0) S_z \\ &\quad + \mathcal{F}_2 S_z [\mathcal{D}^2_{-2,0}(\phi, \theta, 0) + \mathcal{D}^2_{2,0}(\phi, \theta, 0)], \end{aligned} \tag{2}$$

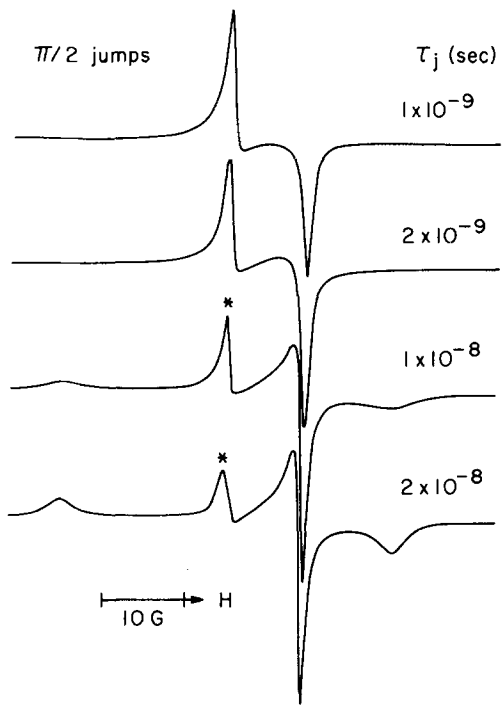

FIG. 18. Theoretical spectra assuming the in-plane $\pi/2$ jumps about the normal to the internuclear axis of O_2^- (y axis) as a function of τ_j, the mean lifetime between jumps. $1/T_1^0 = 0.5$ G was used.

where

$$\mathfrak{F}_0 = \tfrac{2}{3}\left[g_{z'} - \tfrac{1}{2}(g_{x'} + g_{y'})\right]\hbar^{-1}\beta_e \mathcal{B}_0 \tag{3a}$$

and

$$\mathfrak{F}_2 = \frac{1}{\sqrt{6}}(g_{x'} - g_{y'})\hbar^{-1}\beta_e \mathcal{B}_0 , \tag{3b}$$

where the $\mathfrak{D}^2_{K,0}(\phi,\ \theta,\ 0)$ are the Wigner rotation matrix elements with θ the angle between the dc magnetic field and normal to the surface, taken as the axis of rotation, while ϕ is the angle of rotation about this axis. (The prime coordinate system refers to the principal axes of the diffusion tensor, while the unprimed coordinates used until now refer to those of the g tensor. We assume in our models that $g_{z'} = g_y$, $g_{y'} = g_z$, and $g_{x'} = g_x$.) We may write Eq. (2) more explicitly as

$$\mathcal{H}_1(\theta,\ \phi) = \mathfrak{F}_0 \tfrac{1}{2}(3\cos^2\theta - 1)\mathcal{S}_z + \mathfrak{F}_2 \tfrac{1}{2}\sqrt{\tfrac{3}{2}}\sin^2\theta(e^{2i\phi} + e^{-2i\phi})\mathcal{S}_z . \tag{4}$$

We must now take matrix elements of $\mathcal{H}_1(\theta,\ \phi)$ with respect to the planar rotational degrees of freedom, i.e.,

$$\langle m|\mathcal{H}_1(\theta,\ \phi)|m'\rangle = \mathfrak{F}_0 \tfrac{1}{2}(3\cos^2\theta - 1)\mathfrak{M}_s \delta_{m,m'} + \mathfrak{F}_2 \tfrac{1}{2}\sqrt{\tfrac{3}{2}}\sin^2\theta \mathfrak{M}_s \delta_{m',m\pm 2} , \tag{5}$$

where we have also taken matrix elements of $\mathcal{S}_z \to \mathfrak{M}_s$. Now $(g_{x'} - g_{y'}) \approx 2.0271 - 2.0025 = 2.46\times 10^{-2}$, so that $(\hbar/k)\mathfrak{F}_2 \tfrac{1}{2}\sqrt{\tfrac{3}{2}} \approx 3.29\times 10^{-3}$ °K, or a very small perturbation on the rotational states compared to θ_r. Thus (since the $m = \pm 1$ are not allowed by the Pauli exclusion principle), we see that the term in $\mathfrak{F}_2$ would make a negligible contribution to the spectrum *at any temperature*, if the model of free planar rotation were to apply, i.e., virtually complete (quantum mechanical) averaging over ϕ would characterize the ESR spectrum even at 4 °K. This is totally inconsistent with the observations, so we may exclude this limiting case.

Another alternative would be to argue that as the O_2^- rotates in a plane (nearly) parallel to the surface, then it must drag the net surface countercharge due to *lattice polarization* with it. Thus, even in the limit when there is no ϕ-dependent potential to the rotation, there would be an additional inertial drag, which we could formally represent as a renormalized moment of inertia: $\tilde{I} \gg I$. (The possibility of only a small ϕ-dependent potential is consistent with some of the results of the extended Hückel calculations.) Then, to be consistent with our experiments, we must require that $\tilde{\theta}_r \equiv \hbar^2/2\tilde{I}k < 3\times 10^{-3}$ °K, i.e, $\tilde{I}$ must be at least three orders of magnitude larger than I as a result of the inertial drag. In the limit $\tilde{\theta}_r \ll \hbar\mathfrak{F}_2/k$, the rotor will show no quantum effects in the ESR spectrum but would appear to be entirely classical. In order to pick up the incipient quantum effects in this limit, one must first diagonalize the infinite tridiagonal matrix generated by Eq. (5) to obtain the correct zero-order basis functions, and then treat the contributions of Eq. (1b) (but with $I - \tilde{I}$) as the perturbation. Actually, since Eq. (1b) depends on m^2, one could terminate this matrix for $m_n^2 \gg (\hbar\mathfrak{F}_2/k)/\tilde{Q}_r$ with the contributions of Eq. (1b) explicitly included along the diagonal.[54,55] (If m_n^2 is very high, then there will be problems of rotation–vibration coupling as well as some Born–Oppenheimer breakdown, which would tend to reduce the rotational level spacings.)

[It is interesting to note that such a tridiagonal matrix is *formally* (but not physically) identical to the slow-tumbling matrix required for planar rotation, where one replaces im^2R_I in the latter case by $m^2\hbar/2\tilde{I}$ to obtain the effects of coherent quantum mechanical averaging.]

Each resulting eigenfunction will represent a mixed rotational state with its own effective value of the term in $\mathfrak{F}_2\mathcal{S}_z$, i.e., there will be a static distribution of "apparent" values of $\mathfrak{F}_2$ leading to inhomogeneous broadening of the two outer regions of the ESR spectrum. The relative intensity of the nth eigenfunction to the ESR spectrum will be proportional to the equilibrium density matrix element $\langle n|\rho|n\rangle$, where

$$\rho \equiv \exp[-\hbar(\mathcal{H}_r + \mathcal{H}_1)/kT]/Z , \tag{6a}$$

with

$$Z \equiv \mathrm{Tr}\ \{\exp[-\hbar(\mathcal{H}_r + \mathcal{H}_1)/kT]\} \approx \left(\frac{kT\tilde{I}}{2\hbar^2}\right)^{1/2} \tag{6b}$$

and $\mathcal{H}_r = L_z^2\hbar/2\tilde{I}$ is the Hamiltonian operator for the free planar rotor, and we have approximated the partition function Z by that of the classical internal rotor, since the large m states for which $E_m > |\mathfrak{F}_2|$ should dominate the trace. Note that Eq. (6) is defined so that $\mathcal{H}_0$ factors out, since it does not affect this discussion. Thus,

$$\langle n|\rho|n\rangle \cong 1/Z \tag{7a}$$

for eigenstates n formed mainly from free rotor functions ψ_m where $m^2\tilde{\theta}_r/T \ll 1$, while

$$\langle n|\rho|n\rangle < 1/Z \tag{7b}$$

for eigenstates n dominated by ψ_m for which $m^2\tilde{\theta}_r/T \gtrsim 1$. The fact that the population of many eigenstates is proportional to $1/Z$, which is only weakly dependent on T, might well be consistent with the temperature independence of the observed line broadening between 4 and 15 °K, but more detailed calculations would be required.

As the temperature increases and the rotor becomes increasingly affected by the thermal modes (e.g., phonons) on the surface, the rotational states become modulated in a manner described formally by Freed.[56] It is based on solving the quantum mechanical stochastic-Liouville equation for the density matrix ρ, defined for the combined spin and rotational degrees of freedom

$$\dot{\rho} = i[\mathcal{H},\ \rho] - \Gamma_r\rho , \tag{8}$$

where $\mathcal{H} = \mathcal{H}_0 + \mathcal{H}_r + \mathcal{H}_1$ and Γ_r represents the relaxation of the rotational levels by the thermal modes. In the simplest modeling of Γ_r we can introduce $T_{1,r}$'s for the inverse rates of thermally induced rotational transitions and $T_{2,r}$'s for the inverse linewidths of the thermally induced broadening of rotational transitions. Then, as $|\Gamma_r|$ approaches $|\mathfrak{F}_2|$ in magnitude, there will be thermally induced line shape changes, which will act first to broaden the outer regions of the ESR spectrum and then induce a motional narrowing of the spectrum, such that the broadened outer wings approach each other, while the central peak is relatively unaffected. In fact, in the limit $\hbar^2/\tilde{I} \to 0$ we must recover the classical limit. Another way of recovering the classical limit is when the broadening between adjacent (even) m values for the rotor (contained in Γ_r) becomes greater than the separa-

tion between these levels given by $(\hbar/2I)(2m-1)$ for $m \geq 1$.[56] Thus, residual quantum effects on the ESR spectrum could persist from the contributions of the larger m states.

Large barriers to rotation: Suppose, however, we postulate a large barrier to rotation with the C_{4v} symmetry expected for the Ti^{4+} site [cf. Fig. 8(B)]. In this limit the free planar rotor model goes over to torsional oscillations in each of four equivalent potential wells with the possibility of quantum mechanical tunneling between them. Such a model has been discussed in detail for a threefold barrier (i.e., methyl group rotation),[54] but can be rewritten for the present case. One must solve the quantum mechanical equation

$$\mathcal{H}_R \psi(\phi) = E\psi(\phi) , \tag{9a}$$

$$\mathcal{H}_R = -\frac{\hbar^2}{2\tilde{I}} + V(\phi) , \tag{9b}$$

where we shall let $V(\phi) = \frac{1}{2} V_4(1 - \cos 4\gamma)$, where $\gamma = \phi - \alpha$, and is discussed further below. This may be reduced to the Mathieu equation form

$$\frac{d^2M(x)}{dx^2} + [(b - \tfrac{1}{2}s) - \tfrac{1}{2}s\cos 2x]M(x) = 0 \tag{10}$$

by the substitutions

$$2x \equiv 4\phi + \pi , \tag{11a}$$

$$s \equiv V_4/(2\hbar^2/\tilde{I}) , \tag{11b}$$

$$b \equiv E/(2\hbar^2/\tilde{I}) , \tag{11c}$$

the solution of which is well known.[57,58] In the limit of very high barrier, i.e., $s \gg 1$, one obtains the torsional oscillator model, i.e., each torsional oscillator is split into three tunneling levels of A_1, E, and $B_{1\text{or}2}$ symmetry with the E state being doubly degenerate. For the ground oscillator state the lowest level is the A state with $E_A \cong E_{T,0} + 2\Delta_0$, then $E_E \cong E_{T,0}$, and $E_B \cong E_{T,0} - 2\Delta_0$, where

$$\langle H_\nu^{(k)} | \mathcal{H}_R | H_\nu^{(k)} \rangle = E_{T,\nu} = 4\hbar(V_4/2\tilde{I})^{1/2}(\nu + \tfrac{1}{2}) , \tag{12a}$$

$$\langle H^{(k)} | \mathcal{H}_R | H_\nu^{(k')} \rangle = \Delta_\nu , \tag{12b}$$

$k = 1, 2, 3,$ or 4, $\nu = 0, 1, 2, 3, \ldots$, with $k' = 4$ or 2, 1 or 3, when $k = 1$ or 3, 2 or 4, respectively, and $H_\nu^{(k)}$ is the νth harmonic-oscillator function for the torsional motion about the kth minimum. The Pauli exclusion principle applied to $^{16}O_2^-$ prohibits the states of E-type symmetry (i.e., they are odd with respect to rotations of π). Thus, there is a two-level tunneling splitting of $4\Delta_0$ between states of A- and B-type symmetry. They are

$$\psi_{R,A}^{\nu} = \frac{1}{2}\sum_{k=1}^{4} H_\nu \tag{13a}$$

and

$$\psi_{R,B}^{\nu} = \frac{1}{2}\sum_{k=1}^{4} (-1)^{k-1} H_\nu^k . \tag{13b}$$

Following Hecht and Dennison[57] (after converting from a three-well to a four-well problem), we have

$$2\Delta_0' = 7.05 H'^{3/4} \exp(-1.324\sqrt{H'}) , \tag{14a}$$

where

$$H' = 16 V_4/(9\hbar^2/2\tilde{I}) \tag{14b}$$

and

$$\Delta_0' \equiv \Delta_0/(\hbar^2/2\tilde{I}) \tag{14c}$$

valid for large H'. If we assume $E_{T,0} \gg kT$, then only the $\nu = 0$ torsional states would be appreciably populated.

We now need the matrix elements of $\exp(\pm 2i\phi)$ which we first expand about each of the four potential minima at $\phi_1 = \alpha$, $\phi_2 = \alpha + \frac{1}{2}\pi$, $\phi_3 = \alpha + \pi$, and $\phi_4 = \alpha + \frac{3}{2}\pi$ to yield

$$e^{\pm 2i} \cong (-1)^{k-1} e^{\pm 2i\alpha}[1 \pm 2i\gamma_n - 2(\gamma_n)^2 + \cdots] ,$$
$$k = 1, 2, 3, 4, \tag{15}$$

and $\gamma_k \equiv \phi - \phi_k$. Thus, ϕ is used as the axis of internal rotation relative to the azimuthal angle α relating to the orientation of the Ti^{4+} complex on the surface.

We then use the "zero-differential overlap" approximation

$$\langle H_{\nu'}^{k'} | \gamma_k^n | H_{\nu''}^{k''} \rangle \cong \langle H_{\nu'}^{k} | \gamma_k^n | H_{\nu''}^{k} \rangle \delta_{kk'} \delta_{kk''} , \tag{16}$$

and because $E_{T,\nu}$ is taken as very large, only the terms for $\nu' = \nu''$ are nonnegligible. Then we obtain

$$\langle \psi_{R,\nu}^{A} | e^{\pm 2i\phi} | \psi_{R,\nu}^{A} \rangle = \langle \psi_{R,\nu}^{B} | e^{\pm 2i\phi} | \psi_{R,\nu}^{B} \rangle = 0 , \tag{17a}$$

$$\langle \psi_{R,\nu}^{A} | e^{\pm 2i\phi} | \psi_{R,\nu}^{B} \rangle = \langle \psi_{R,\nu}^{B} | e^{\pm 2i\phi} | \psi_{R,\nu}^{A} \rangle^* = e^{\pm 2i\alpha}(1 - 2\bar{\phi}_\nu^2) \equiv e^{\pm 2i\alpha} u_\nu , \tag{17b}$$

where

$$\bar{\phi}_\nu^2 = (\nu + \tfrac{1}{2})\beta \tag{18a}$$

and

$$\beta = 2\hbar^{-1}(2V_4\tilde{I})^{1/2} . \tag{18b}$$

These results are consistent with the B-type symmetry of $e^{\pm 2i\phi}$.

To obtain the isolated rotator average over ϕ one must now solve the 2×2 matrix

$$\begin{array}{c} \\ A \\ B \end{array} \begin{pmatrix} E_{T,\nu} + 2\Delta_\nu & t_\nu \\ t_\nu & E_{T,\nu} - 2\Delta_\nu \end{pmatrix} , \tag{19a}$$

where

$$t_\nu = \mathfrak{F}_2 \sqrt{\tfrac{3}{2}}(\sin^2\theta \cos 2\alpha) u_\nu M_s \tag{19b}$$

and one must then perform classical averaging over θ and α representing the random distribution of orientations of the Ti^{4+} complexes. In the limit $|t_\nu| \ll 4|\Delta_\nu|$ the eigenvalues to second order become

$$E_{T,\nu} + 2\Delta_\nu + t_\nu^2/4\Delta_\nu \cong E^A \tag{20a}$$

and

$$E_{T,\nu} - 2\Delta_\nu - t_\nu^2/4\Delta_\nu \cong E^B , \tag{20b}$$

and the A and B states are approximately decoupled with a small residual spectral contribution from $\mathfrak{F}_2$ given by $\pm t_\nu^2/4\Delta_\nu$) and this is *not* consistent with our observations. The opposite limit of $|\mathfrak{F}_2| \gg 4|\Delta_\nu|$, which would be more consistent with our experimental observations, is more complex to treat because the $\sin^2\theta\cos 2\alpha$ function has

zeros at $\theta = 0$ or π and $\alpha = \pi/4$ or $3\pi/4$. Thus, this peculiar case allows for large quantum effects for these orientations (i.e., the spectral components from these orientations, for which $\mathcal{F}_2$ is very small, will experience quantum mechanical averaging) while there would be largely classical behavior for the other orientations. For these other orientations, which are actually the important ones spectrally (i.e., the $\theta = \pi/2$ and $\alpha = 0$ or $\pi/2$ orientations dominate the outer wings), the zero-order eigenfunctions and eigenvalues to second order are $\frac{1}{2}(\psi^A_{R,\nu} \pm \psi^B_{R,\nu})$ and $\pm(t_\nu + 2\Delta_\nu^2/t_\nu)$, respectively.

We do note that, for $E_{T,0} \gg kT$, only the ground torsional states are populated, so that the only significant quantum effect on the outer spectral regions will be the effect of the correction term $\pm 2\Delta_0^2/t_0$. A possible broadening mechanism could then be the existence of some small site-to-site variation in V_4, which by Eq. (14) can lead to large variation in Δ_0.

As the temperature increases, the contact with the thermal modes increases, and relaxation effects begin to play a role in the ESR spectrum. Again this type of problem has been discussed in detail. One must again solve the density matrix equation [Eq. (8)]. In this limit we note that when $|\Gamma_R| \gg |4\Delta_\nu|$, i.e., when the thermal broadening of the hindered rotational levels is greater than the torsional splitting between A and B levels, formally classical line-broadening results are obtained,[54–56] although peculiar model dependence could still be present which may not be adequately represented by simple classical models. We do wish to note that the classical-limiting model is that of jumps between the four equivalent positions and we have clearly noted that it is inconsistent with our ESR observations. Also, we would expect, in the classical limit, that such jumps exhibit a substantial activation energy!

Isotope effects: We now wish to consider the effects of isotopic substitution. For the mixed isotopes $^{17}O-^{18}O^-$ there are no longer any restrictions from the Pauli exclusion principle, so that in the case of a "free rotation" model all eigenfunctions of $m = 0, \pm 1, \pm 2, \pm 3, \ldots$ are allowed. Except for the contribution of the $m = \pm 1$ levels,[54] no substantial change in observables would be expected from the presence of odd rotational levels which are separately coupled by the $\mathcal{F}_2$ term. In the case of the "torsional oscillator" model there would now be all three torsional levels of symmetry A, E, and B, so that instead of Eq. (19) one would need to solve a 4×4 matrix. In neither case would two spectra be expected from $^{17}O-^{18}O^-$ purely from these symmetry considerations.

However, if the two oxygens were in inequivalent positions (as expected from the two ^{17}O hf splittings observed), then the resulting moments of inertia in the two isotopic cases would be slightly different but could still have a substantial effect on Δ_0 due to the exponential dependence of Eq. (14). This could then be the source of different broadening of the different hf components.

The case of $^{17}O-^{17}O^-$ is one of a pair of fermions. Here we must first classify the symmetry of the nuclear spin states $[(2I+1)^2 = 36$ states] according to the C_2 operation equivalent to permutation of the ^{17}O nuclei. In the case of free rotation the even (odd) m states combine only with nuclear spin states of odd (even) symmetry with respect to C_2. In the case of the torsional oscillator model the torsional A and $B(E)$ states combine only with nuclear spin states of odd (even) symmetry with respect to C_2. Again no substantial changes in observables would be expected for the former model, while for the latter the behavior of the degenerate E states must be considered.

In any event, our isotopic spectra including a rich mixture of the various isotopic species were not well enough resolved for careful line shape studies.

7. Other models

We wish to point out other models which we believe should be considered to try to improve the agreement with the experimentally observed spectra. We have seen that a small jump (Brownian) model consistently gave the best fit at low (high) temperatures, while a coherent four-jump model was inappropriate. This latter is the model one obtains in the limit of a very high fourfold barrier. It may be that the explicit use of a relatively low fourfold barrier for a Brownian rotation model would be better in that it would only be a perturbation on models that are at least partially satisfactory and this perturbation might be more jump like at the lower temperatures.

Another model, which would emphasize the drag effect of the surface polarization charge, would be a slowly relaxing local structure (SRLS) model,[15,59] in which the O_2^- molecule rotates relative to a fluctuating potential due to thermal fluctuation in this surface polarization charge. While we suggest these as classical models, they are actually contained as special cases within the general types of quantum models we have already obtained. The extent to which classical models will prove satisfactory vs the need for quantum corrections is a question requiring further exploration, as we have already noted. We also recall the classical model suggested in Sec. III. C. 5 of the addition of a wobble degree of freedom, which would also have a quantum counterpart.

In our consideration of classical models, we have, so far, ignored a proper inclusion of inertial effects, i.e., the gaslike motion of a nearly free internal rotor. While this might seem a plausible model for O_2^- adsorbed on a surface, we do wish to note that previous simulations of inertial effects on slow motional ESR spectra[60] using a planar type of model demonstrated that there is a pronounced sharpening of spectral features rather than the smearing out of features noted in our present experiments. This sharpening of spectral features was attributed to the simple periodicity of the planar rotations. (The approximate free diffusion model used in our simulations was shown *not* to have these characteristics because of its oversimplified nature,[60] but is found useful from the point of view of diagnosing spectral trends.) Thus, we do not believe that inertial effects *per se* can improve our spectral fits.

8. O_2^- on Ti/Vycor vs on Ag/Vycor

Clarkson and Kooser[4] investigated slow molecular motion of O_2^- stabilized on metallic Ag supported on Vycor by means of saturation transfer (ST) ESR. They compared the ST–ESR spectra with the theoretical ones calculated using simple Brownian and strong jump isotropic rotational models, and concluded that the Brownian model seemed to fit the experimental spectra better. Furthermore, they mentioned that the rotational correlation times between about 2×10^{-4} sec (173 °K) and 10^{-6} sec (273 °K) correspond well to a Langmuir type of dwell time τ, i.e., the mean time the O_2^- spends at a particular adsorption site. We estimate from their very limited data an activation energy of order 6 kcal/mole, which is much greater than the value of 0.5 kcal/mole that we observe for O_2^- on Ti/Vycor.

Since the ESR analysis of Clarkson and Kooser was a simple one (i.e., they did not consider any motional anisotropy or moderate types of jump, they neglected any hfs contribution due to Ag, and they assumed axial symmetry of the g tensor), it did not permit a rigorous comparison between predicted and observed spectra. It nevertheless appears that the spectra do not have the very anisotropic type of motion we have observed.

For these reasons we conclude that the nature of the motions in the two cases are quite different. We believe the differences can be understood as follows: First, the g values for O_2^- on Ag/Vycor are characteristic of O_2^-(I) (cf. Table II), which we have found in our Ti/Vycor studies to show no appreciable motional effects over a wide temperature range, and it appears to be a more stable and more strongly bound species. Thus, for the Ti/Vycor samples containing only small amounts of Ti (0.2 wt%), the *partially* reduced Ti atoms are probably complexed into the silica structure [cf. Figs. 8(A) and 8(B)] and relatively far apart. Thus, the only dynamical process(es) we detect is that of O_2^-(III) rotating with respect to a fixed Ti site in a planar motion, the activation energy for hopping between different Ti sites being too high. This planar motion, especially if nearly barrier free, is then expected to (and does) show a small activation energy. The O_2^-(I) on Ag/Vycor may also be characterized by being orientationally restricted when bound to a particular Ag^+ atom. However, if, as Clarkson suggests, the O_2^- is formed on the metal surface, it is possible to have a migration of the O_2^- (with the positive counter charge) along the surface. Rotational averaging would then occur because translation of O_2^- on the Ag metal surface would allow it to sample a range of orientations of the surface relative to the lab frame. Such a hopping of O_2^- between adjacent Ag atoms with virtually the same orientation would require large translational excursions to achieve appreciable reorientation, and this is just the simple Brownian limit for the rotational reorientation. Also, such a hopping between Ag atoms would be expected to have a substantially higher activation energy than for the nearly unhindered motion [of O_2^-(III) at a single site].

IV. CONCLUSIONS

We wish to make the following points:

(1) Of the several types of O_2^-, the stable species O_2^-(III) exhibits highly anisotropic motion on Ti supported on porous Vycor glass as well as on other surfaces. The more stable species O_2^-(I) does not appear to exhibit such motional effects.

(2) This highly anisotropic motion is well approximated by planar rotational diffusion about an axis perpendicular to the O_2^- internuclear axis and parallel to the normal to the surface.

(3) The higher temperature spectra, while not adequately fit in detail by any of the simple models considered, nevertheless yields a rather small activation energy of 0.5 kcal/mole characteristic of a not very hindered motion.

(4) The lower temperature spectra are reasonably (but not exactly) fit by a classical model of small-jump diffusion, but below 15 °K the motion becomes temperature independent. This strongly suggests coherent quantum mechanical motional averaging of the spectrum. There must also be strong interaction with the surface, probably due to the strong surface polarization charge, which can lead to a "renormalized" moment of inertia that is much larger than that for gaseous O_2^- and/or an orientation-dependent effective potential.

(5) The possibilities of residual quantum effects on the temperature-dependent dynamics as well as further refinements in the classical-limiting models are worthy of further investigation in view of the well-resolved experimental spectra, anomalous isotope effects, and the great sensitivity of the simulated spectra to the details of the model.

ACKNOWLEDGMENTS

We wish to thank Dr. C. T. Yu, Dr. M. Nilges, and Dr. G. Barkley for their help and advice. This research was supported by Grant No. DE-ACO2-80ER04991-A002 from the Office of Basic Energy Sciences of the DOE, by NSF Grant CHE 77-26996, by the Cornell Materials Science Center (NSF), and acknowledgment is made to the Donors of the Petroleum Research Fund, administered by the American Chemical Society, for partial support (Grant No. 10935-NS).

[1]For example, see the recent review by I. B. Afans'ev, Russ. Chem. Rev. **48**, 527 (1980) and references therein.
[2]R. J. Kokes, *International Congress on Catalysis* (North-Holland, Amsterdam, 1974), 3rd edition, p. 484.
[3]For references before 1972, see J. H. Lunsford, Catal. Rev. **8**, 135 (1973); for references after 1973, see J. C. Vedrine, Abstracts of the IV Special Colloque Ampere, Leipzig, 1979, p. 21; for recent reports, see, for example, K. Aika and J. H. Lunsford, J. Phys. Chem. **82**, 1794 (1978); M. Iwamoto, Y. Yoda, N. Yamazoe, and T. Seiyama, *ibid.* **82**, 2565 (1978); M. Iwamoto and J. H. Lunsford, Chem. Phys. Lett. **66**, 48 (1979); J. R. Katzor, G. C. A. Schut, and J. H. C. Van Hooff, J. Catal. **59**, 278 (1979).
[4]R. B. Clarkson and R. G. Kooser, (a) Surf. Sci. 74, 325 (1978); (b) Varian Application Note EPR-77-2, Varian Associates (1977).
[5]C. M. Muha, J. Phys. Chem. **71**, 633, 640 (1967).
[6]G. B. Garbutt, H. D. Gosser, and M. Fujimoto, J. Chem. Phys. **48**, 4605 (1968).

[7]M. Iwaizumi, S. Kubota, and T. Isobe, Bull. Chem. Soc. Jpn. **44**, 3227 (1971).
[8]T. Komatsu and A. Lund, J. Phys. Chem. **76**, 1727 (1972).
[9]M. Shiotani, F. Yuasa, and J. Sohma, J. Phys. Chem. **79**, 2669 (1975).
[10]J. Sohma and M. Shiotani, *Magnetic Resonance in Colloid and Interface Science*, ACS Symposium Series No. 34, edited by H. A. Resing and C. G. Wade (American Chemical Society, Washington, D.C., 1976), p. 141.
[11](a) T. M. Pietrzak and D. E. Wood, J. Chem. Phys. **35**, 2454 (1970); (b) Recently, we observed temperature-dependent ESR spectra of NO_2 adsorbed on Vycor glass surfaces in the temperature range of 4.2 to 220°K. The spectra have now been analyzed using our slow motional ESR spectral theory. We have found that the rotational motion of NO_2 is axially symmetric about its y axis (the O–O direction) below 77°K and the rotational diffusion about the axes perpendicular to the y axis is negligible. Furthermore, it was found that the rate of rotational diffusion about the y axis increases with increasing temperature (below 77°K) and also that about the normal to the the y axis increases with temperature above 77°K. Almost isotropic rotational diffusion is estimated for the spectra at and above 185°K. These results are quite different from those of the NO_2/zeolite system reported by Pietrzak and D. E. Wood. The details will be published (M. Shiotani and J. H. Freed).
[12]S. Schlick and L. Kevan, (a) J. Phys. Chem. **83**, 3424 (1979); (b) J. Chem. Phys. **72**, 784 (1980); (c) J. Am. Chem. Soc. **102**, 4622 (1980).
[13](a) S. A. Goldman, G. V. Bruno, C. F. Polnaszek, and J. H. Freed, J. Chem. Phys. **56**, 716 (1972); (b) J. H. Freed, *Spin Labeling: Theory and Applications*, edited by L. Berliner (Academic, New York, 1976), Vol. 1, Chap. 3.
[14]J. S. Hwang, R. P. Mason, L. P. Hwang, and J. H. Freed, J. Phys. Chem. **79**, 489 (1975).
[15]C. F. Polnaszek and J. H. Freed, J. Phys. Chem. **79**, 2283 (1975).
[16]R. F. Campbell and J. H. Freed, J. Phys. Chem. **84**, 2668 (1980).
[17](a) S. Alexander, A. Baram, and Z. Luz, Mol. Phys. **27**, 441 (1974); (b) A. Baram, Z. Luz, and S. Alexander, J. Chem. Phys. **64**, 4321 (1976).
[18]R. B. Clarkson and A. C. Cirillo, Jr., (a) J. Vac. Sci. Technol. **9**, 1073 (1972); (b) J. Catal. **33**, 392 (1974).
[19]V. A. Shvets and V. B. Kazansky, (a) J. Catal. **25**, 123 (1972); (b) Kinet. Catal. (USSR) **12**, 834 (1971).
[20]The authors are indebted to Mr. George Ramseyer of Cornell University for determining the Ti concentration using an Atomic Absorption Spectrophotometer.
[21](a) M. Nilges, M. Shiotani, C. T. Yu, G. Barkley, Y. Kera, and J. H. Freed, J. Chem. Phys. **73**, 585 (1980); (b) J. H. Freed, DOE Reports No. COO-4991-1 (1979) and COO-4991-2 (1980).
[22]A. I. Mashchanko, V. B. Kazansky, G. B. Pariiskii, and V. M. Sharapov, Kinet. Catal. (USSR) **8**, 725 (1967).
[23]C. Naccache, P. Moriandeau, M. Che, and A. J. Tenche, J. Chem. Soc. Faraday Trans. 2 **67**, 506 (1971).
[24]P. Meriandeau and J. C. Vedrine, J. Chem. Soc. Faraday Trans. 2 **72**, 472 (1976).
[25]M. Iwamoto, Y. Yoda, N. Yamazoe, and T. Seiyama, J. Phys. Chem. **82**, 2564 (1978).
[26]W. Känzig and M. H. Cohen, Phys. Rev. Lett. **3**, 509 (1959).
[27]M. Anpo, C. Yun, and Y. Kubokawa, J. Catal. **61**, 267 (1980).
[28]C. Naccache, Chem. Phys. Lett. **11**, 323 (1971).
[29]Recently, we were able to directly determine the T_1 and T_2 by means of electron–spin echoes (ESE). $T_1 = 1.5\ (\pm 0.5) \times 10^{-4}$ sec and $T_2 = 4(\pm 1) \times 10^{-6}$ sec were obtained on the central portion of the spectrum (corresponding to $g_y = 2.0092$) at 4.2°K. The T_2 obtained from ESE is about 10 times longer than that derived from the linewidth of the cw-ESR spectrum. This indicates that the linewidth of the central band (0.2 G) originates from inhomogeneous broadening. Moreover, it was found that the T_2 (ESE) was almost constant between 4.2 and 18°K, then decreases gradually with increasing temperature. This result is consistent with the present cw-ESR observation of a temperature-independent line shape below 15°K. Details will be published (M. Shiotani, L. J. Schwartz, A. E. Stillman, and J. H. Freed).
[30]A. Kazusaka, L. K. Yong, and R. F. Howe, Chem. Phys. Lett. **57**, 592 (1978).
[31]A. J. Tench and P. I. Holroyd, Chem. Commun. **1968**, 471.
[32]A. J. Tench and T. Lawson, Chem. Phys. Lett. **8**, 177 (1971).
[33]P. Meriandeau, C. Naccache, and A. J. Tench, J. Catal. **21**, 208 (1971).
[34]M. Che, I. F. J. Kibblewhite, A. J. Tench, M. Dufaux, and C. Naccache, J. Chem. Soc. Faraday Trans. 1 **69**, 857 (1973).
[35]Y. B. Taarit and J. H. Lunsford, J. Phys. Chem. **77**, 780 (1973).
[36]M. Che and A. J. Tench, Chem. Phys. Lett. **18**, 199 (1973).
[37]M. Che, C. Naccache, and A. J. Tench, J. Chem. Soc. Faraday Trans. 1 **70**, 265 (1974).
[38]M. C. R. Symons, J. Phys. Chem. **76**, 3095 (1972).
[39]The authors would like to acknowledge Dr. M. Nilges for supplying the rigid limit simulation program written for the PDP-11 computer. Note that, in the program, the second-order perturbation of a spin Hamiltonian reported by J. A. Weil [J. Magn. Reson. **18**, 113 (1975)] was used.
[40]K. Tatsumi, M. Shiotani, R. Hoffmann, and J. H. Freed (to be published). For the extended Hückel MO calculation, a C_{4v} summetry was assumed at the Ti^{4+} site. Using the constant bond distances of $d_{Ti-O} = 1.944$ Å, $d_{O=O} = 1.44$ Å, and $d_{Ti-O_1} = 1.83$ Å, spin densities, charges on atoms, and total energy were calculated as a function of rotation angles α and β and displacement of Ti^{4+} from the plane [cf. Fig. 8(BII)].
[41]R. H. Silsbee, J. Phys. Chem. Solids **28**, 2525 (1967).
[42]Based on the assumption of $A_\perp = 0$, the spin densities were derived from the magnetic parameters listed by B. A. Goodman and J. B. Raynor, Adv. Inorg. Chem. Radiochem. **13**, 135 (1970).
[43]Note that H. Kon [J. Am. Chem. Soc. **95**, 1045 (1973)] observed an isotope effect between ESR spectra of $^{16}O-^{16}O$ and $^{18}O-^{18}O$ ($S = 1$) in a few matrices (N_2, Ar, CO, and Xe) at temperatures below 10°K, which was explained in terms of torsional oscillation of O_2 in the matrix around the equilibrium position.
[44]R. P. Mason and J. H. Freed, J. Phys. Chem. **78**, 1321 (1974).
[45]W. Känzig, J. Phys. Chem. Solids **23**, 479 (1962).
[46]H. R. Zeller and W. Känzig, Helv. Phys. Acta **40**, 845 (1967).
[47]R. T. Shuey and H. R. Zeller, Helv. Phys. Acta **40**, 873 (1967).
[48]R. Pirc, B. Zeks, and P. Gosar, J. Phys. Chem. Solids **27**, 1219 (1966).
[49]P. H. Kasai, J. Chem. Phys. **43**, 3322 (1965).
[50]J. H. Lunsford, in Ref. 3.
[51]J. C. Vedrine, in Ref. 3.
[52](a) R. F. Campbell, E. Meirovitch, and J. H. Freed, J. Phys. Chem. **83**, 525 (1979); (b) The convention $K \geq 0$ for Eqs. (5) in that article (52a) could cause some misunderstanding. It is preferable to consider the variables $C^{L\pm}_{K,0}$ to be defined for both positive and negative values of the K index, satisfying the relation $C^{L\pm}_{-K,0} = (-1)^K C^{L\pm}_{K,0}$. Therefore, in the evaluation of the matrix elements only the positive K values are needed since this equation allows one to replace the $C^{L\pm}_{|K|1,0}$ by $(-1)^K C^{L\pm}_{|K|1,0}$.
[53](a) R. H. Silsbee[40] pointed out that two types of reorientation took place for O_2^- in KI, one a 60° reorientation, the other a 90°, in the temperature range of 4.2 from 1.5°K; (b) Recently, S. Schlick and L. Kevan reported that the temperature-dependent ESR spectra of trimethyl peroxy radical,[12(a)] peroxide $(CO_2-O_2)^-$ on MgO surface,[12(b)] and peroxy polyethylene radical (Ref. 12(c)) in urea–polyethylene complex were successfully simulated assuming 120° jumps (for the former two systems) and 180° jumps (for the latter system) of the O–O

group around the C–O bond. The agreement with experiment seems to us to be reasonable, although differences in detail suggest that the motion may have additional complicating features.

[54]We have not included the spin–rotational interaction in Eqs. (2)–(5), although, in principle it should appear. For our planar model we should get an additional secular contribution to Eq. (5) of $mC_{g'g'}\cos\theta\,\mathfrak{m}_s\delta_{mm'}$, which could only affect the central line, and would thus not be expected to contribute to the observed broadening. In fact, if we use: $\mathbf{C} = -2\mathbf{A}\cdot\Delta\mathbf{g}$ [cf. P. W. Atkins in *Electron-Spin Relaxation in Liquids*, edited by L. T. Muus and P. W. Atkins (Plenum, New York, 1972), Ch. XI], where $\mathbf{A}$ is the rotational tensor and $\Delta\mathbf{g} = \mathbf{g} - g_e\mathbf{1}$, then we find $\mathbf{C}_{g'g'} \approx 2.8\times10^{-2}$ °K, while the renormalized $\tilde{I}$ would yield $\tilde{C}_{g'g'} \lesssim 4.2\times10^{-5}$ °K $\ll \hbar\mathfrak{I}_2\sqrt{\frac{3}{2}}/2k$.

[55]Some general aspects of quantum-classical correspondence for planar rotors are discussed by R. Liboff [Found. Phys. **5**, 271 (1975)].

[56](a) J. H. Freed, J. Chem. Phys. **43**, 1710 (1965); (b) J. H. Freed, J. Chem. Phys. **45**, 1251 (1966); (c) J. H. Freed, in *Electron Spin Relaxation in Liquids*, edited by L. T. Muus and P. W. Atkins (Plenum, New York, 1972), Chap. IX.

[57]K. T. Hecht and D. M. Dennison, J. Chem. Phys. **26**, 31 (1957).

[58]C. C. Lin and J. D. Swalen, Rev. Mod. Phys. **31**, 841 (1959).

[59]A. E. Stillman and J. H. Freed, J. Chem. Phys. **72**, 935 (1980).

[60]G. V. Bruno and J. H. Freed, J. Phys. Chem. **78**, 935 (1974).